Journal of Structural Geology 33 (2011) 1237–1253

Contents lists available at ScienceDirect

Journal of Structural Geology

journal homepage: www.elsevier.com/locate/jsg

Insights into fluid flow and water-rock interaction during deformation of carbonate sequences in the Mexican fold-thrust belt

Elisa Fitz-Diaz*, Peter Hudleston, Luc Siebenaller, David Kirschner, Antoni Camprubí, Gustavo Tolson, Teresa Pi Puig

UNAM, Instituto de Geología, Av Universidad #3000, CU 04510 Coyoacan, Mexico, DF, Mexico

ARTICLE INFO

Article history:
Received 22 December 2010
Received in revised form
15 May 2011
Accepted 28 May 2011
Available online 23 June 2011

Keywords:
Fluid flow
Fold-thrust belt
Fluid inclusion
Stable isotope
Carbonate platform
Illite-smectite

ABSTRACT

Analysis of mesoscopic structures and related veins allows the history of deformation and role of fluids to be established for part of the central Mexican Fold-Thrust Belt (MFTB). The MFTB developed in mostly carbonate rocks with prominent lateral facies changes associated with two platforms and two basins. Fluids played a key role in the deformation, both physically and chemically, by reducing strength and inducing extensional fracturing through raised pore pressure and by providing the medium for solution transfer on the grain-scale. Veins preserve portions of water related to deformation as fluid inclusions. Lithology and lithological variations strongly control deformation styles, with thrusts dominant in the platforms and folds dominant in the basins, and also influence fluid behavior by controlling both porosity and permeability. Structural observations allow distinguishing veins (dominantly calcite) of several generations, emplaced early, during and late/after deformation (V1–V3 respectively). $\delta^{13}C$ and $\delta^{18}O$ analyses in calcite from veins and host rock show that the veins confined within thrust slices are isotopically buffered by the host rock and differ in isotopic composition from veins emplaced along major thrusts or crosscutting thrust slices. δD analyses in fluid inclusions and clay minerals strongly suggest rock interaction with meteoric fluids in the west (hinterland) and with fluids close to SMOW in the less deformed eastern (foreland) side of the cross-section. By focusing on a single stratigraphic interval exposed across the width of the fold-thrust belt, we propose a conceptual model that explains the differences in vein-rock isotopic composition, the differences of in isotopic composition of aqueous fluids active during deformation, and the progression of clay dehydration reactions as being related to variations in temperature and intensity of deformation in a growing tectonic wedge.

1. Introduction

It seems likely that fluids significantly influence the mechanical processes, deformation mechanisms and chemical reactions that operate in fold-thrust belts. Fluid pressure has been invoked to reduce frictional resistance on a basal *décollement* zone and on major thrusts, following Hubbert and Rubey, (1959), and in general its role has been evaluated for reducing stresses required for Coulomb failure in major fault zones and fold-thrust belts (Davis et al., 1983; Dahlen et al., 1984; Dahlen, 1990; Sleep and Blanpied, 1992; Byerlee, 1993). Investigations in active accretionary prisms show the intermittent passage of fluids along faults and fractures on a human time-scale (e.g., Von Huene and Lee, 1982; Davis et al., 1983; Moore et al., 1991; Byerlee, 1993; Saffer and Tobin, 2011). On a longer time-scale, the results of such intermittent fluid flow may be recorded in veins and rocks in older fold-thrust belts formed either subaqueously or subaerially (e.g., Ramsay, 1980; Rye and Bradbury, 1988; Vrolijk et al., 1988; Fisher and Byrne, 1990; Fisher and Brantley, 1992; Moore and Vrolijk, 1992). Structural and textural features of syntectonic veins should be able to provide us with valuable information on fluid transport mechanisms and fluid–rock interaction during deformation (Ramsay, 1980; Fisher and Brantley, 1992; Bons et al., 2000; Oliver and Bons, 2001).

In fold-thrust belts, veins can grow at different stages of development of the local host structures with which they are associated. Such veins can be formed in an open system if their minerals precipitate from external fluids passing though fracture networks or along fault surfaces during deformation, with a limited interaction with the host rock (e. g., mobile hydrofractures, Bons, 2001 and Oliver and Bons, 2001); or in a closed system, if they are the result of extensive fluid–rock interaction through pressure-solution and solution transfer mechanisms (Durney, 1972; Rutter,

* Corresponding author. Tel.: +52 55 56224308.
E-mail address: fitzde@gmail.com (E. Fitz-Diaz).

0191-8141/$ – see front matter © 2011 Elsevier Ltd. All rights reserved.
doi:10.1016/j.jsg.2011.05.009

1983; Engelder, 1984) at the grain-scale within the rock mass. Whether the veins formed in an open or a closed system is strongly controlled by lithology and lithological variations, since mineralogy and fabric of rocks determine primary porosity and permeability at the grain-scale (Schmoker and Gautier, 1989; Bjørlykke et al., 1989; Bjørlykke, 1997). Lithology also plays a primary role in controlling the style of deformation in a fold-thrust belt (e. g., brittle vs. ductile or thrust-dominated vs. fold-dominated, Fitz-Díaz et al., 2011), and on a broader scale the style of deformation affects the porosity and permeability of the rock, either by opening channels by fracturing or by sealing them with impermeable rocks or cements growing during folding and thrusting.

In this study we investigate fluid flow and water–rock interaction along a transverse section of a thin-skinned thrust belt, the Mexican Fold-Thrust Belt (MFTB). This section was selected because: (1) it is well exposed and well studied (Suter, 1987; Carrillo-Martínez, 1989, 1990; Fitz-Díaz et al., 2011, in press; Ortega-Flores, 2011); (2) it is dominated lithologically by Cretaceous carbonates, (3) it contains large-scale lateral facies variations, in the form of basins and platforms, providing a striking contrast in deformation style (km-scale structures dominated by thrusts in the platforms vs. meso-scale structures dominated by folds within the basins); and (4) the presence of fluid during deformation is indicated by calcite veins emplaced along major thrusts, and by several generations of veins formed in association with smaller thrusts and folds within thrust slices. By studying the veins, the host rocks and structures, we can gain information about fluid–rock interaction at the grain-scale and how this might vary in space and time in an evolving fold-thrust belt wedge, and also about fluid flow and storage throughout the belt and how these might be controlled by the major lithological variations associated with the platforms and basins.

Our strategy is to combine structural, petrographic and geochemical analyses of minerals and fluids in order to obtain information on: (1) the temperature during deformation; (2) fluid flow and fluid–rock interaction during deformation; and (3) the possible sources of fluids active during the deformation. Much of the earlier work on the origin and role of fluids in the development of structures has focused on the scale of individual folds or thrusts (Fyfe and Kerrich, 1985; Cox et al., 1987, 2007; Grant et al., 1990; Foreman and Dunne, 1991; Kirschner et al., 1993; Crispini and Frezzotti, 1998; Hodgkins and Stewart, 1994; Kirschner and Kennedy, 2001; Richards et al., 2002; Hilgers et al., 2006; Fischer et al., 2009) (Travé et al., 2007; Sample, 2010). In this study we elucidate key aspects of fluid flow on the scale of a heterogeneous fold-thrust belt as a whole, by focusing on a single stratigraphic interval that is exposed across the width of the fold belt.

2. Geological framework

The Cordilleran Orogen extends along the western margin of North America and is the result of accretionary processes (Coney et al., 1980; Coney and Evenchick, 1994) related to subduction from Jurassic to Early Cenozoic times (Armstrong, 1974; DeCelles, 2004; Evenchick et al., 2007). In the internal (western) part of the Cordillera, accretion of allochthonous terranes (Coney et al., 1980; Campa-Uranga, 1983), magmatism and metamorphism were the dominant geological processes. In the external (eastern) part, however, shortening in the rocks of the autochthonous sedimentary cover associated with deformation at very low metamorphic grade prevailed. The eastern part of the Cordillera constitutes the Rocky Mountain Fold-Thrust Belt (RMFTB), which has its southern counterpart in the MFTB (Fig. 1).

In the study area the MFTB is only 125 km wide, and the deformed rocks are dominantly carbonates. Sedimentary and stratigraphic studies in the area (Imlay, 1944; López-Ramos, 1983;

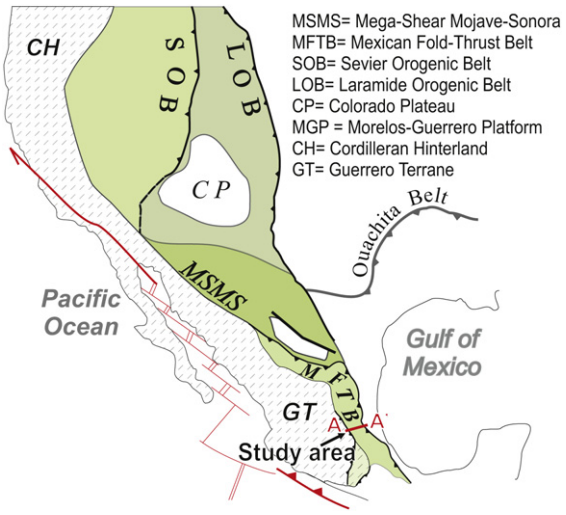

Fig. 1. Generalized tectonic map of the Cordilleran Orogenic Belt showing the tectonic setting of the Mexican Fold-Thrust Belt (MFTB) and the location of the study area in Central Mexico.

Suter, 1980, 1984, 1987; Valencia-Islas, 1996; Carrillo-Martínez et al., 2001), indicate that the sedimentary sequence is determined by four paleogeographical elements: two thick carbonate platforms, El Doctor Platform (EDP), about 1 km thick, and the Valles-San Luis Potosí Platform (VSLPP), about 2.5 km thick; and two thinner packages of basinal carbonates, regionally known as the Zimapán Basin (ZB) and the Tampico-Misantla Basin (TMB, Fig. 2). The two platforms consist of Neocomian-Cenomanian thickly bedded to massive wackestones, packstones and rudstones with abundant fragments of mollusks and benthic foraminifera. The basins are characterized by sections of 300–700 m thick Berriasian-Cenomanian thinly bedded limestones, interbedded with thinner shale, bentonite and chert layers. Details of the stratigraphy can be found in Suter (1987).

The MFTB shows all the elements of an orogenic wedge (Davis et al., 1983). It is thin-skinned, wedge shaped, tapering to the east (Fig. 2), and the gradient of deformation increases toward the back of the wedge (Fitz-Díaz et al., 2011). The detachment separates a deformed sedimentary cover from an undeformed crystalline basement in the front of the cross-section (eastwards). The stratigraphic changes within the sedimentary cover play a major role in how the deformation is accommodated within the wedge, and in the evolution of the fold-thrust belt.

Deformation in the platforms is dominated by thrusts and fault-related folds at a kilometer scale (e. g. Fig. 3a), and by fractures, veins and stylolites at a mesoscopic scale. In contrast, the deformation in the basins is more ductile and is dominated by mesoscopic buckle folds with a strong axial plane pressure-solution cleavage and fold-related veins that are pervasive throughout the cross-section (Fig. 3b–d), although thrusts are also present within the basins.

Analysis of structures on a mesoscopic scale is presented in Fitz-Díaz et al. (in press). The spatial-temporal variations of upright chevron folds that characterize the two basins indicate two stages of fold growth: the first one by buckling, which accounted for 45–55% of the shortening, followed by a second one of flattening that contributed up to 20% shortening, to produce a total shortening of 65–75%. Folds in the Tampico-Misantla Basin show a gradient of deformation that varies from 20% at the front of the basin to 65% near its western boundary (Figs. 2 and 3c). The folds in the Zimapán Basin accumulated an overall shortening of 70–75%,

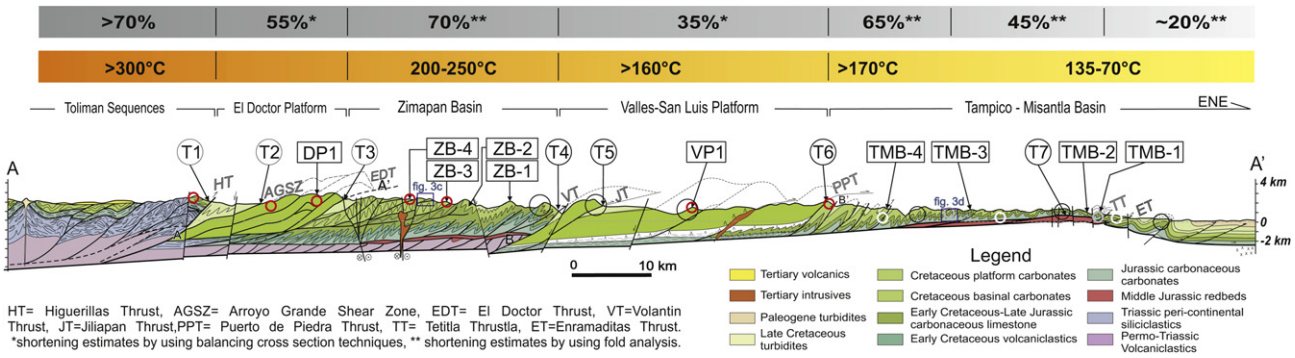

Fig. 2. Geological cross-section along the line A–A′ in Fig. 1. The sampling localities are projected onto the line of section. Locality code: T = major thrusts; ZB = in Zimapan Basin; TMB = in Tampico-Misantla Basin; DP = in El Doctor Platform; PV = in Valles-San Luis Potosi Platform. Estimates of shortening and temperature of deformation are indicated in the gray and orange bars above the cross-section, and indicate averages and ranges for particular segments, respectively. Circles indicated localities where samples for thermometric estimates were taken: red circles = microthermometry of fluid in this study; black circles = temperature of homogenization reported by Gray et al. (2001); gray circles = illite crystallinity; and white circles = vitrinite reflectance reported by Ortega-Flores (2011). (For interpretation of the references to color in this figure legend, the reader is referred to the web version of this article.)

with variation within the basin and the highest amounts at the margins (Figs. 2 and 3d).

Another prediction of the orogenic wedge theory is that rocks exposed to the rear of a wedge are subjected to deeper and therefore higher temperature and pressure conditions than the rocks exposed at the front. So it happens in the MFTB, where temperature has been determined by microthermometry of fluid inclusions (Gray et al., 2001, and new data in this paper), illite crystallinity, and vitrinite reflectance (Valencia-Islas, 1996; Ortega-Flores, 2011). Such data show a gradient in the thermal conditions of deformation from about 80 °C in the front of the MFTB to about 190 °C on the western boundary of the Tampico-Misantla Basin, 200–250 °C in the Zimapán Basin, and more than 300 °C in the rocks of the carbonates in the western extreme of the cross-section (Fig. 2).

3. Methodology

3.1. Timing of deformation events and veins

The overall wedge shape of the MFTB is inferred from surface mapping and borehole data, and various section-balancing techniques (Fitz-Díaz et al., 2011) were applied to produce the section shown in Fig. 2. Two main phases of deformation (D1 and D2) affected the rocks of the fold-thrust belt (Fitz-Díaz et al., in press), D1 being the major event that produced thrusts, folds, and a penetrative axial planar cleavage (S1) in pelitic units (Trancas, Soyatal and Santiago formations). D2 modified the D1 structures to produce open folds, and a crenulation cleavage (S2) affecting the S1 cleavage. D2 is the only event that affected Paleogene sequences in the easternmost part of the section. Through a careful structural-kinematic analysis we distinguish veins emplaced before, during and after the main shortening event (D1). In the platforms, scarce millimeter-size veins (V0) formed parallel to diagenetic stylolite surfaces, and are perpendicular to stylolite average surfaces (and bedding). No preferred orientation in strike was detected in these veins. Early veins (V1) are strongly affected by folding and shear; they are named V1a when they are emplaced between strata and V1b when they are oblique to bedding. The former are present anywhere in the cross-section and the latter are common in the basinal carbonates (Fig. 3b–e). Syn-tectonic veins (V2) helped to accommodate local extension around the hinges of folds and shear in the limbs of flexural folds during D1 within limestone layers; depending on the timing of their emplacement, they are named V2a (en echelon arrays in the limbs of flexural folds, Fig. 3d and close-up in 3f), or V2b (dominantly extensional veins perpendicular to bedding in attenuated limbs of flattened folds in the TMB, Fig. 3c). When indistinguishable they are simply labeled as V2. V3 veins postdate V2, are entirely made up of calcite, almost vertical and crosscut many layers (Fig. 3c). They typically show blocky textures (Fig. 3g).

3.2. Sampling strategy

3.2.1. In major thrusts

Based on observations of fluid passage along thrusts in active accretionary prisms (Von Huene and Lee, 1982; Saffer and Tobin, 2011), we test the idea that major thrusts in the MFTB represent channel ways for fluids escaping during deformation. If the rocks affected by thrusting are carbonates with characteristic $\delta^{13}C$ and $\delta^{18}O$ values (around 0‰ with respect to the PDB standard, unaltered by deformation) fluids with a different isotopic composition circulating through the fault zones would likely leave a distinct isotopic imprint in recrystallized and new calcite formed during deformation (Kirschner and Kennedy, 2001). To investigate this, we took samples along profiles centered at each thrust 'plane' and extending into the hangingwall and footwall (Fig. 3a). Sample spacing was closer in the fault zone and wider outwards, extending far enough away from the fault to identify a pre-deformation signature that can be used as reference (Fig. 3a). 209 samples of limestone, cataclasites and veins were collected in seven localities, T1–T7 (see Figs. 2 and 3 and Table 1 for location and Appendix 1 for descriptions). The samples were prepared to allow for more detailed structural observations at a small scale and the selection of material for geochemical and isotopic analyses. About 5 mg of powdered sample was obtained by micro-drilling every significant feature on each hand sample. Micro-sampling was normally done at the center of calcite veins and on calcite megacrystals, carefully avoiding inclusions of other minerals and rock fragments. Sampling of carbonate rocks was done in homogeneous cement-rich areas and fossils shells. In fault rocks, micro-samples were taken in different shear domains (micro-breccia with veins, fault gouge, cataclasite or calci-mylonite). However, some of these domains (e.g. pink iron oxide-rich cataclasites) could not be analyzed because they are poor in calcite (see Appendix 1).

3.2.2. In mesoscopic structures

Outcrops showing evidence for local, meter scale (e.g. Fig. 3b–d) to grain-scale deformation and clear vein crosscutting relationships

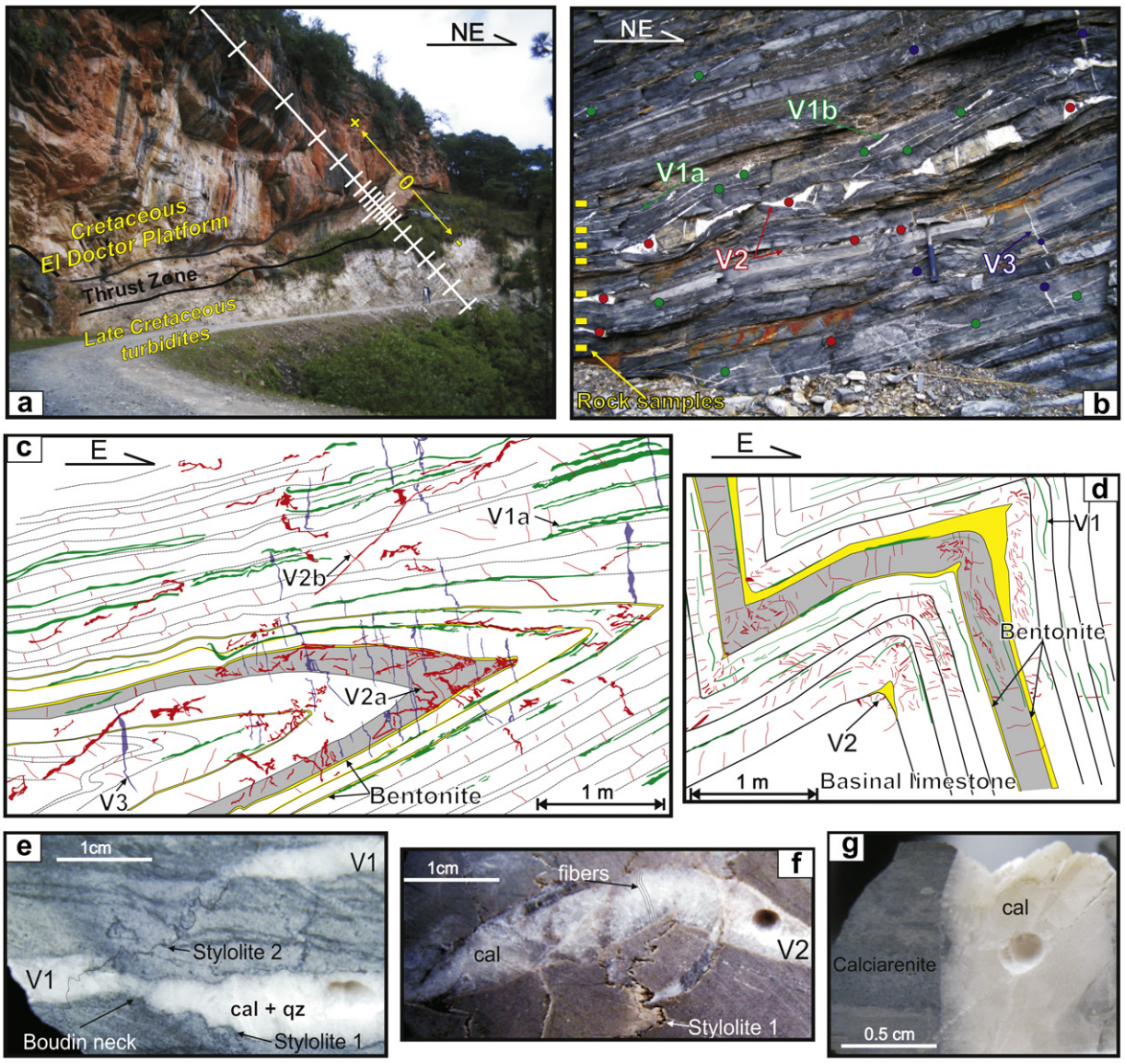

Fig. 3. Photographs and sketches of selected outcrops. (a) El Doctor Thrust, showing how sampling was carried out for stable isotope analysis. (b) Different generations of fold-related veins in outcrop. (c) and (d) Distribution of different generations of fold-related veins in mesoscopic folds in the middle of the Zimapán and Tampico-Misantla basins, respectively. (e) Sawn surface of V1a vein emplaced in carbonaceous mudstone; it is boudinaged and affected by two generations of stylolites (stylolite 1parallel to bedding and 2 parallel to the axial plane of folds). (f) V2a vein confined in a wackestone layer, cutting a stylolite parallel to bedding. (g) cut surface of V3 showing a granular texture. The vein generations in a–d are color coded (green for V1, red for V2 veins and blue for V3). (For interpretation of the references to color in this figure legend, the reader is referred to the web version of this article.)

were selected for study. The sites are located within thrust slices in the platforms and basins (Fig. 2, Table 2). Fig. 3c and d show the distribution and abundance of fold-related veins in two well exposed outcrops in the Zimapán and Tampico-Misantla Basins. Fig. 3e and f, show examples of cut surfaces of V1 and V2 where the micro-samples were taken. In both we observe the same generations of veins associated with folds, except that in the ZM they are modified by further flattening that occurred in a more evolved stage of folding. We believe the structures in these two outcrops, while individually distinct, represent different stages of progressive development of folds in comparable lithologies in the basinal strata.

For $\delta^{13}C$ and $\delta^{18}O$ analyses in calcite, 5–8 samples of host rocks were obtained, in continuous stratigraphic columns starting at over 20 cm from veins and shear zones to ensure isotopic preservation (see Fig. 3b), These samples were taken from the centers of individual limestone layers in order to avoid contamination. At least 5 samples from every vein generation (see Fig. 3b) were taken. The amount of sample at every site allowed testing for homogeneity and ensured that statistically representative values for the host rocks and each generation of veins were obtained. A total of 209 samples were taken for $\delta^{13}C$ and $\delta^{18}O$ analyses at the various localities (see Figs. 2 and 3 and Table 1 for location and Appendix 2 for details of samples).

3.2.3. Mineralogical and fluid inclusion analyses

δD_{water} was analyzed in fluid inclusions from vein calcite and quartz. For this purpose, single crystals of these minerals were separated from different vein generations from six localities. In addition, 16 illite/smectite-rich clay samples for δD analyses were collected from bentonite layers in five outcrops (TMB1, TMB3, ZB2–ZB4).

To assess the temperature of formation of the veins, 14 samples were collected for microthermometry of fluid inclusions. The

Table 1
List of samples and analytical methods applied.

Sampling Locality	Paleogeographical Element	Coordinates (UTM)		Analysis			
		Latitude	Longitude	$\delta^{18}O$ & $\delta^{13}C$ in calcite	δD in fluid inclusions	δD in Illite-Smectite	clay analysis
T1	Tolimán Sequences, Higuerillas Thrust	2327861	414409				
T2	EL Doctor Plat., western boundary	2310383	429611				
T3	ZB, western boundary, El Doctor Thrust	2306474	438744				
T4	Zimapán Basin, eastern boundary, Volatín Thrust	2316548	459120				
T5	Valles-SLP Platform, Jiliapan Thrust	2320090	463823				
T6	Tampico-Misantla Basin, western boundary, Puerto de Piedra Thrust	2327403	488033				
T7	TMB, detachment zone	2324707	517033				
TMB1	Tampico-Misantla Basin	2334710	519126				
TMB2	Tampico-Misantla Basin	2340418	513206				
TMB3	Tampico-Misantla Basin	2334457	504135				
TMB4	Tampico-Misantla Basin	2331187	494461				
VP1	Valles-San Luis Potosí Platform	2325153	468068				
ZB1	Zimapán Basin	2318737	453221				
ZB2	Zimapán Basin	2309151	454054				
ZB3	Zimapán Basin	2311027	449760				
ZB4	Zimapán Basin	2311201	441909				
DP1	EL Doctor Platform	2312661	429611				

Microthermometry of fluid inclusions in quartz from syntectonic veins.
The type/s of analysis carried on the samples taken in each locality.

samples come from syntectonic (V2) calcite and quartz veins emplaced in chert layers in outcrops ZB3 and T1.

3.3. Illite-smectite characterization

The bentonite samples were prepared following the recommendations of the IGCP 294 IC working group (Kisch, 1990). An unaggressive procedure was used for clay separation, which included: rock crushing, dispersion of powder in de-ionized water in an ultrasonic probe, separation of the fraction <2 μm by gravity settling, washing and concentration by centrifugation, and finally preparation for X-ray diffraction (XRD) by sedimentation onto round glass slides. The coarse, medium and fine clay fractions were not separated, since we assume that clay minerals in bentonite are authigenic and therefore that different size fractions do not differ in their clay mineralogy. The concentration of the suspension was controlled to make sure that the weight of clay in the dried slide exceeded 2.5 mg/cm^2. The measurements were done in a Shimadzu XRD-6000 diffractometer, with a voltage of 40 kV and a filament current of 30 mA, using CuKα radiation and a graphite monochromator. The clay samples were analyzed by XRD in air-dried form, saturated with ethylene glycol (EG) and when the clay samples were heated at 550 °C. All the preparations were measured over a 2θ angle range of 2–70 ° (air-dried) and 2–40 ° (glycolated and heated) in steps of 0.02 ° and 2 s integration time. The profiles were analyzed using Shimadzu software. Illite crystallinity (IC) was measured using FWHM (full-with-half maximum) parameter of the 10 Å illite peak on oriented clay preparation of the <2 μm fraction (Kübler, 1967, 1968; Kübler and Jaboyedoff, 2000; Warr and Rice, 1994) and expressing the results in terms of the Bragg angle 2θ.

Illite identification and the percentage of smectite in mixed illite/smectite layers were estimated by using the methods described by Srodon (1984), Srodon and Eberl (1984), Reynolds (1992) and Moore and Reynolds (1997). The Ir index (Srodon and Eberl, 1984) was calculated by comparing the intensity ratio (peak height ratio) of the 001 and 003 reflections from the air-dried and the glycolated samples. Peak positions (d-spacing) were standardized against the quartz 100 peak taken at 4.26 Å.

In order to obtain statistically representative IC values, duplicates were analyzed for all samples. All the measurements were done under the same analytical conditions and calibrated using international reference materials (NIST 675 and NIST 640d). No inter-laboratory standardization procedure was done (as suggested by Warr and Rice, 1994) since the purpose of this paper is to observe variations of IC values rather than to obtain the absolute values.

Table 2
Structural, textural and compositional variations among the different generations of veins. E = extensional, S = shear veins, SE = dominantly shear and some extensional veins, ES = dominantly extensional and some shear veins; b = blocky, be = blocky elongate, f = fibrous texture, c = crustiform, bd = banded. Cal/Qz (%) = rough estimate of percentage of calcite in proportion to quartz in the veins per weight. This was determined in few samples by comparing the weight of the vein with the weight of quartz after removing calcite with diluted HCl.

Vein type	Location	Typical			Cal/Qz (%)
		Length	Width	Texture	
V1-E	TMB	cm-m	1–3 cm	b,be	>95
V1-E	VSLPP	cm-m	1–3 cm	b, be	~100
V1-E	ZB	cm-m	1–3 cm	be, f, b	>85
V1-ES	EDP	cm-m	1–3 cm	b, be	~100
V1a-E	ZB	cm-m	1–3 cm	f, be, b	>80
V1b-S	ZB	5–30 cm	0.5–2 cm	be, b	>90
V2-SE	TMB	1–10 cm	0.5–3 cm	be, f, b	~100
V2-S	VSLPP	cm-m	1–5 cm	b, be	~100
V2a-SE	ZB	1–10 cm	1–3 cm	be, b	>85
V2b-E	ZB	1–30 cm	1–3 cm	f, be, b	>85
V3-ES	ZB	3-x m	0.5–10 cm	c, bd	~100
V3-E	EDP	3-x m	1–20 cm	b, c	~100

3.4. Fluid inclusions

Two types of analysis were carried out on fluid inclusions: microthermometry and δD in inclusion water. For microthermometric analysis, 14 double polished thin sections were prepared of syntectonic calcite and fibrous quartz veins emplaced in chert bands. In 4 of them (2 from each T1 and ZB3 localities) homogenization temperatures (Th) were obtained. Ice melting temperatures (Tmi) were obtained from fluid inclusions trapped in quartz fibers from the ZB3 locality. Workable fluid inclusions are scarce and display diameters ~10 μm. Primary (formed during the grain growth) and secondary fluid inclusion associations (along late micro-fractures) were selected for microthermometry (Fig. 4) by

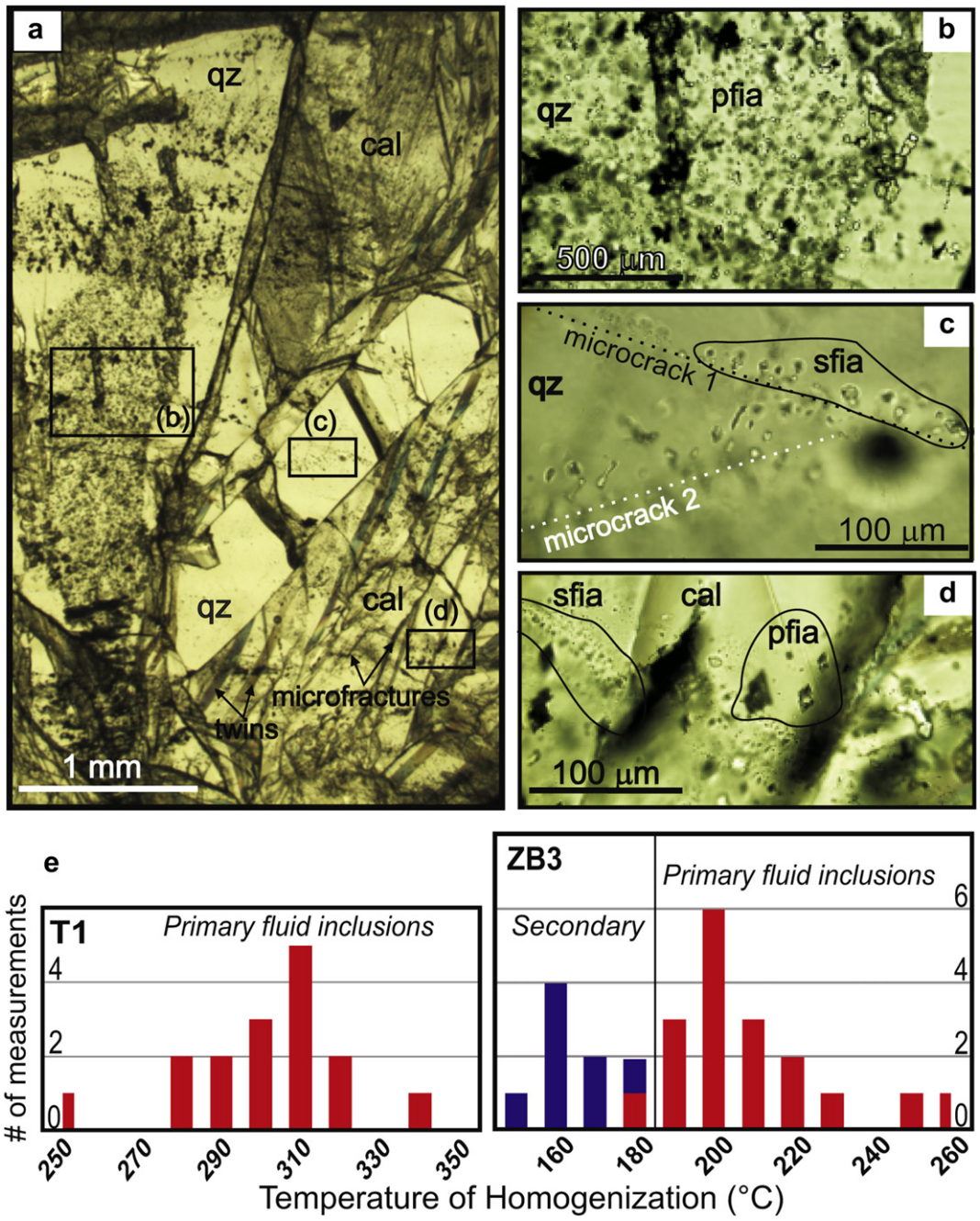

Fig. 4. Fluid inclusions in veins. (a) Quartz and calcite fibers in a V2 vein where the distribution of primary fluid inclusion associations (pfia) is shown in an internal zone of an euhedral quartz crystal, and the secondary fluid inclusion associations (sfia) are hosted along fracture planes. (b) Close-up showing random distribution of pfia in quartz. (c) Closer view of micro-fractures hosting several small secondary inclusions. (d) pfia and sfia in a calcite fiber. Notice the difference in size and abundance of the primary and secondary fluid inclusions. (e) Histograms showing temperatures of homogenization in primary and secondary fluid inclusions in syntectonic veins from localities T1 and ZB3.

using the criteria of (Goldstein and Reynolds, 1994; Touret, 2001; Fig. 4a). The primary inclusions are typically distributed in growth zones in quartz fibers (Fig. 4b) and in clusters in calcite. Primary fluid inclusions are less abundant but bigger than secondary fluid inclusions. Secondary fluid inclusions are typically distributed along micro-fractures that cut quartz crystals and calcite twins (see examples in Fig. 4b–d). Inclusions showing evidence for necking, leakage, and other post-trapping modifications were identified and not used for microthermometry (Goldstein and Reynolds, 1994). Th and Tmi were obtained using a Linkam THMS 600 thermal stage (at the Instituto de Geología, UNAM), with a precision of ±0.2 °C and ±2 °C at low and high temperature determinations, respectively. Salinities were calculated with the equations of Bodnar and Vityk (1994).

3.5. Stable isotope analysis

3.5.1. $\delta^{13}C$ and $\delta^{18}O$ analyses in carbonates

Powder samples of limestone, vein calcite and fault rock were analyzed in a Micromass Isoprime mass spectrometer (at Stable Isotope Lab, Saint Louis University) to determine their $\delta^{13}C$ and $\delta^{18}O$ compositions. Samples of about 0.5–1 mg were made to react with H_3PO_4 at 90 °C for at least 1 h prior to analysis. One in-house

standard was analyzed for every five unknowns. The in-house standard values of $\delta^{13}C = 2.33‰$ and $\delta^{18}O = 24.72‰$ were calibrated against NBS-19 standard values of 1.95‰ and 28.64‰, respectively. The standard deviations of in-house standards in individual sets of analyses (generally 30 analyses for each set) were 0.02–0.08‰ for $\delta^{13}C$ and 0.10–0.15‰ for $\delta^{18}O$.

3.5.2. δD analyses in illite/smectite

Analyses of δD in phyllosilicates were made with an ultra-high temperature Eurovector system (HT-PyrOH) connected to a Micromass Isoprime mass spectrometer (at the Stable Isotope Lab, Saint Louis University). Less than 1 mg of sample or standard was loaded into a silver capsule and pyrolized at 1800 °C in a carbon reaction tube. Liberated gas was separated in a heated GC column and admitted online into the spectrometer. International (NBS22, NBS30) and in-house standards (coumarin, urea, kaolinite) were analyzed before, during, and after the analyses of the unknowns with standard deviations of <2‰ after correcting for sample-size effects and "stretch".

3.5.3. δD analyses in fluid inclusions

For δD analyses in fluid inclusions, calcite was separated from quartz. 3–5 g of calcite were handpicked under a petrographic microscope. Quartz (0.5–2 g) was then separated from the leftover material by dissolving the remaining calcite with 10% diluted HCl in iterative steps. Fluids were then extracted from the inclusions by decrepitation, at 400 °C for calcite and 600 °C for quartz, in a closed cryogenic system. Samples of inclusion water that decrepitated at 100 °C step heating intervals were also collected: from 200° to 400 °C for calcite and from 200° to 600 °C for quartz. The purpose of step heating was to look for isotopic differences in inclusions decrepitating at different temperatures. Bulk H_2O was trapped in Pyrex tubes. H_2O and CO_2 from water and hydrocarbon-bearing fluid inclusions (Appendix 2) were separated following the methodology of Vennemann and O'Neil (1993) and were also trapped in Pyrex tubes. Once these were sealed the pipes were inserted into a muffle furnace at 500 °C for 15 min prior to mass-spectrometric analysis. δD analyses were done on a Finnigan Mat-Delta S mass spectrometer equipped with a dual inlet system (reference gas and sample). In-house, MOW and LIPE standards were used for corrections. These analyses were done in the Stable Isotope Lab at the University of Lausanne.

4. Results

4.1. Structural analysis

The veins in the major thrust zones are most diverse texturally (Table 2), and are always calcite rich. Some are affected by faulting, while others are unaffected and are distributed in *en echelon* arrays that are kinematically consistent with the displacement on the fault. There are also veins with calcite megacrystals that cut cataclastic fabrics and the previous veins. These three groups of veins are early, contemporaneous and late with respect to the displacement that generated the main fabric in the fault.

In both basins there are extensional veins emplaced along the bedding (V1a) and veins oblique to bedding that predate folding (V1b; Fig. 3b–d). These are subsequently folded or sheared, and at a grain-scale they are affected by pressure-solution, as evidenced by two generations of stylolites (one parallel to bedding and another oblique that cuts the first one; Fig. 3e). V1a veins are formed essentially of calcite and quartz in fibrous and elongate-blocky fabrics, in the terminology of Bons et al. (2000). V1b veins typically exhibit blocky and elongate-blocky textures, and are dominantly (>85%) formed by calcite. Most of the V1 veins are affected by micro-fractures, twins (types II and III of Burkhard, 1993) and crystal-plastic deformation. These veins are more abundant in the Zimapán Basin than in the Tampico-Misantla Basin (Fig. 3c and d, Table 2).

V2 veins were characterized through a comparative analysis of fold-related veins from the less folded parts of the front of the MFTB to the highly deformed westernmost areas, along the same stratigraphic unit (Tamaulipas Fm.). V2 veins cut stylolites parallel to bedding and are not commonly affected by S1, in contrast to the V1 veins (Fig. 3f). These veins are commonly found in the outer arcs of buckle folds hinges accommodating extension (e. g. V2a in ZB), and in *en-échelon* arrays, accommodating local shear zones around folds (e.g. V2 in TMB, Fig. 3d). They exhibit fibrous, blocky elongate and blocky textures, and the crystals show late deformation as microfractures and (in calcite) deformation twins (Type II and III of Burkhard, 1993). V2a and V2b vein generations are observed in both basins; however, in the ZB they are affected by slight folding or stretching, which might have happened during a late flattening stage of deformation. In the most evolved folds in the ZB we also see veins accommodating extension in attenuated limbs of flattened folds (V2b, Fig. 3b and c). V2 veins typically show planar vein-rock interfaces, are confined to one or a few strata (Fig. 3f). They are almost 100% calcite when emplaced in limestones, and quartz contents increase (up to 15%) in veins hosted by sandstones or chert. Late veins (V3) are less abundant than V1 or V2 (Fig. 3c and d, Table 2) and are better developed on the western side of the study area (DP and ZB). They are commonly meter-spaced, vertical, several meters long, and unconfined to specific layers. They are made up of reddish semitransparent calcite, commonly with "dog tooth" crystals in open spaces. In other cases they show banded or crustiform textures with variegated coloring.

4.2. Clay analysis

Bentonite layers may constitute up to 20% (to the east of the cross-section AA') of the total thickness of the carbonate series. On the other hand, XRD analyses in the basinal limestone layers indicate that the amount of clay in them is negligible.

Interbedded shale and bentonite are rich in illite-smectite and quartz, have minor amounts of kaolinite, and may also have chlorite and K-feldspar. These were not sampled, to avoid contamination due to authigenic-detrital phase mixing (Srodon et al., 1992). We assume that illite in the bentonite samples was produced from smectite during diagenesis or deformation as indicated in other studies (Weaver et al., 1979; Compton et al., 1999; Abdioglu and Arslan, 2005). X-Ray diffraction patterns of the clay fraction indicate that mixed-layer clays are mostly illitic.

Illite crystallinity (IC) and Ir index vary regionally and range from 0.23 to 1.5 and 0.87 to 6.80, respectively: low illite crystallinity (small IC values) and higher smectite content (high Ir) were found toward the front of the cross-section whereas high illite crystallinity and almost pure illite (low Ir) occur at the back of the tectonic wedge.

4.3. Microthermometry of fluid inclusions

In T1, the homogenization temperatures (Th) measured in primary fluid inclusion assemblages range from 280° to 350 °C, and in ZB3 they range from 180° to 230 °C (Fig. 4). The Th in secondary fluid inclusion assemblages in ZB3 average 160 °C (Fig. 4e). Such temperatures are consistent with those reported by Gray et al. (2001). The temperature of ice melting of primary fluid inclusions in quartz from veins in ZB3 ranges from −4.5 ° to −5.2 °C, and calculated salinities range from 7.17 to 8.14 wt. % NaCl equiv.

Fluid inclusions in syntectonic veins in the Zimapán Basin belong to the H_2O–NaCl system, as extraction of water in a cryogenic system (for δD analysis) produced tiny amounts of CO_2 and no residual gases were detected after isolating water and CO_2. However, hydrocarbons and probably N_2 occur in fluid inclusions from V1 and V2 veins in the Tampico-Misantla Basin. CO_2 from fluid inclusions was analyzed in 2 samples (Appendix 2) and their $\delta^{13}C_{VPDB}$ composition (−34 to −6‰) suggests the presence of hydrocarbons.

4.4. Stable isotope geochemistry

4.4.1. In major thrusts

In Fig. 5 the $\delta^{13}C$ and $\delta^{18}O$ isotopic values are plotted vs. distance across fault zone for all sampling localities. In the two westernmost locations, T1 and T2, veins in the fault zone show distinctly lower values of $\delta^{18}O$ (10–15‰) than rocks in the hangingwall and footwall (18–25‰). In contrast, in the other locations to the east, T3–T7, $\delta^{18}O$ values range from 24 to 27‰ and are the same in fault zone and host rock. These values are typical for Cretaceous carbonates (Weissert et al., 1998; Ferket et al., 2003; Weissert and Erba, 2004). The locations that show the least variation in $\delta^{13}C$ across fault zones are T1, T4 and T7; these are on the east sides of the westernmost unit of the cross-section and the two studied basins (Fig. 2). By contrast, along the thrusts on the western boundaries of the two basins (T3 and T5) $\delta^{13}C$ values are as low as −5‰. These low values might be due to hydrocarbon circulation along these faults. Similar low values, with some variation, are observed in the hangingwall, veins and cataclasites at T5, on the western side of the Valles-SLP Platform. Even lower values (about −15‰), with much variation, occur at T2 on the western side of the El Doctor Platform in both the footwall platform carbonates and the fault rocks. Fluid inclusions with hydrocarbons in veins (V1 and V2) have been observed and have also been reported by Gray et al. (2001) in the TMB.

4.4.2. In mesoscopic structures

In Fig. 6, $\delta^{18}O$ is plotted vs. $\delta^{13}C$ for veins and host limestones in the two basins and platforms. In the two basins, values of both $\delta^{18}O$ and $\delta^{13}C$ in the V1 and V2 veins and host rocks are very similar. In the western platform (DP1), the values of the two isotopes are also very similar for host rocks and V1 and V2 veins, but the values for V3 veins are different. In the eastern platform (Valles-SLP Platform), by contrast, there is more variation and most V1 and V2 veins have significantly lower values of ^{18}O and ^{13}C than does the host rock.

4.4.3. Clays and fluid inclusions

δD values in clay range from −41 to −72‰ (Fig. 7a). They are higher on the eastern side of the cross-section than in the west. A similar

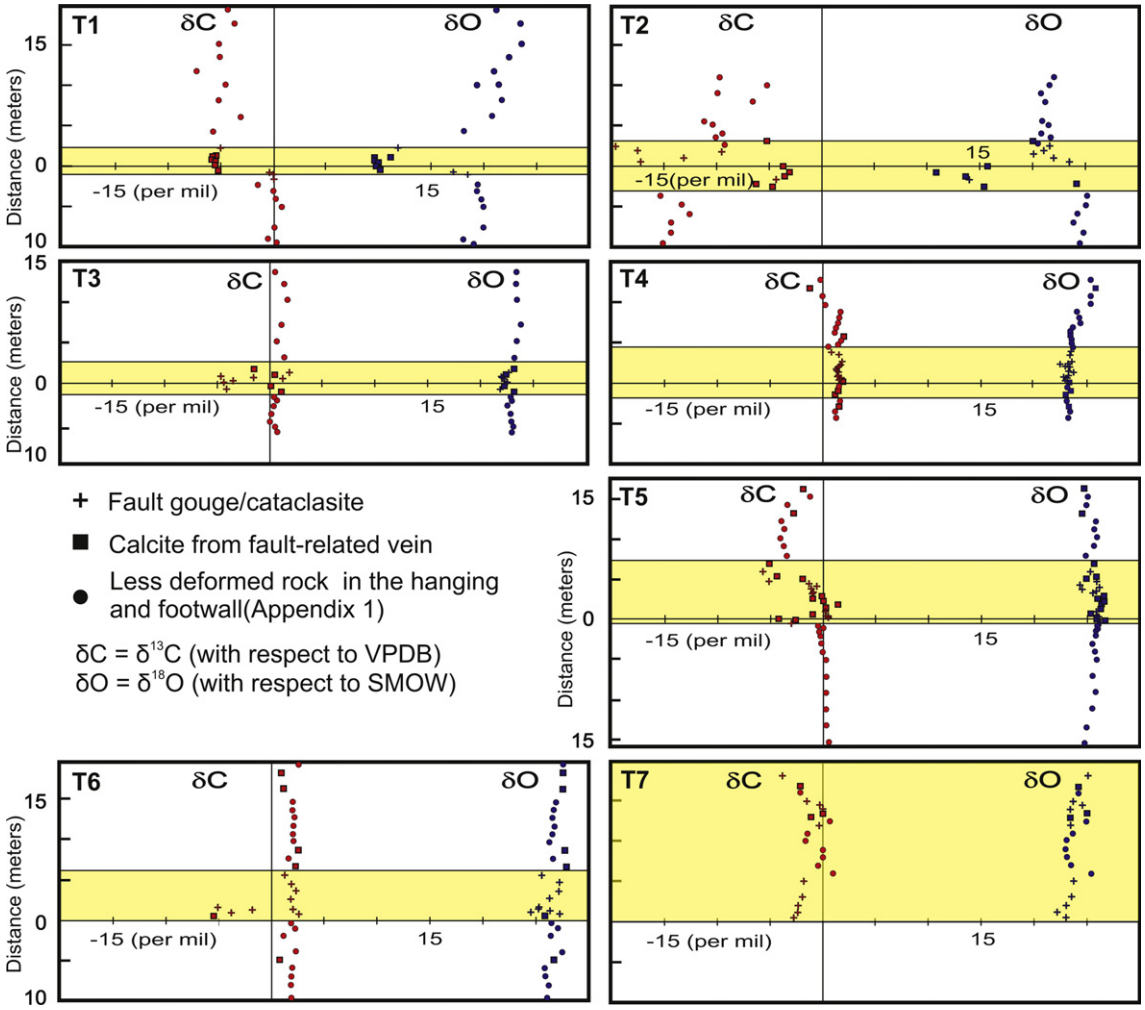

Fig. 5. $\delta^{18}O_{VSMOW}$ and $\delta^{13}C_{VPDB}$ determinations in calcite veins, cataclasites and surrounding carbonate rocks along seven transects across major thrusts (as indicated in the upper left of each diagram). The isotopic values (‰) are plotted against distance, with the origin at the center of the most highly deformed part of the thrust zone (the highlighted area). Sample locations are identified on Fig. 2.

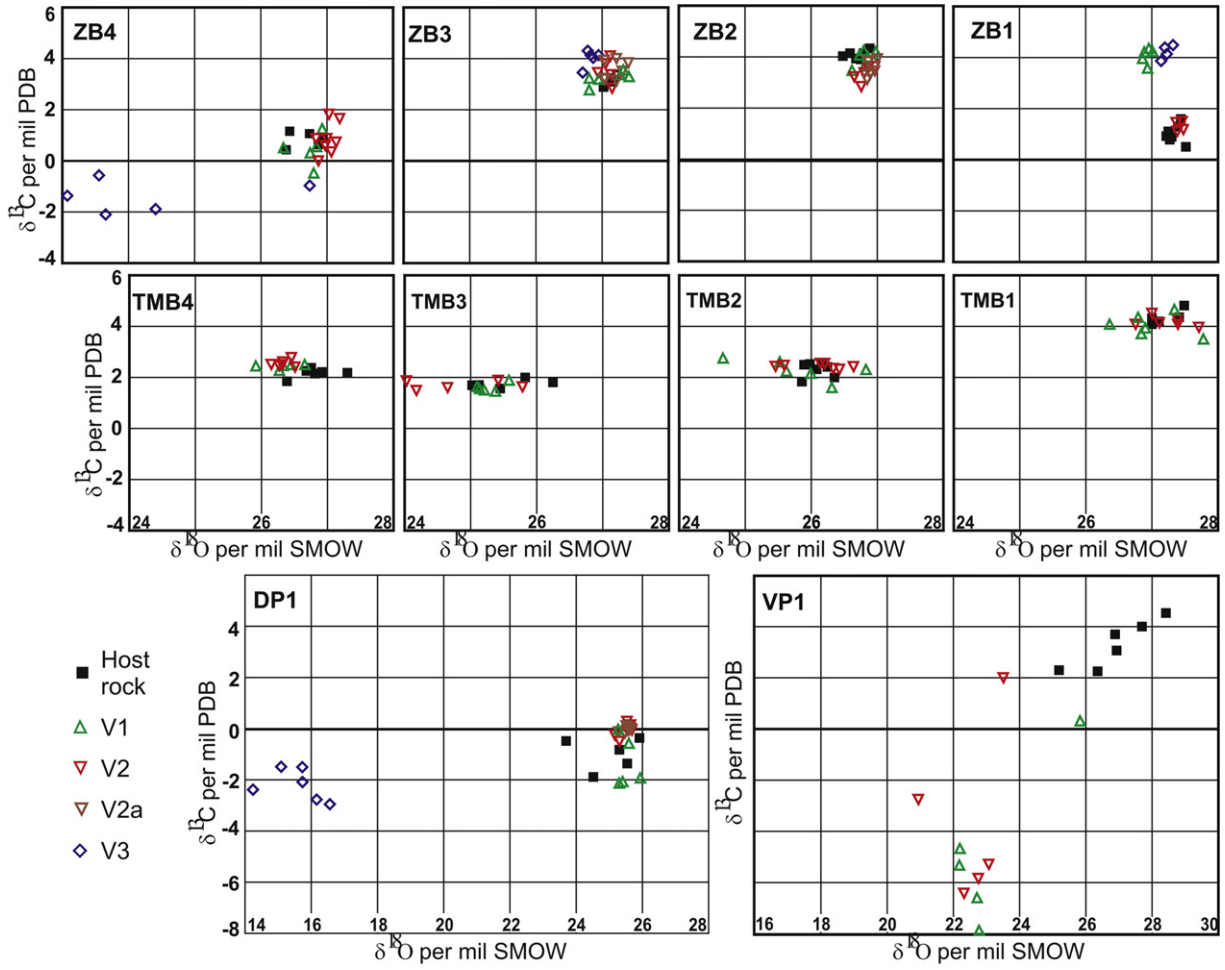

Fig. 6. $\delta^{18}O_{VSMOW}$ vs. $\delta^{13}C_{VPDB}$ in calcite from limestones and fold-related veins V1–V3 veins in ten different outcrops, keyed on the upper left of each diagram. V1 and V2 have $\delta^{18}O$ and $\delta^{13}C$ signatures close to their host rock, 24–28‰, and −1–4‰, respectively, except for locality VP1. V3 veins in ZB4 and ED1 are strongly depleted in ^{18}O and slightly depleted in ^{13}C, while V3 veins in ZB1 are enriched in ^{13}C with respect to the host rock.

trend is observed for inclusion water from V1 and V2 veins, with the range of values being broader for V1 (0 to −61‰ Fig. 7a) than for V2 (−33 to −58‰), and with a large overlap with the range for clays. The lowest values of δD among the veins are for V3 (−60 to −70‰).

5. Interpretation

5.1. Wedge mechanics as deduced from vein analysis

The presence of veins of different generations in the MFTB is evidence for fluids operating at different scales throughout the deformation history. Vein types relate to fracture modes (e. g., mode I-extensional or mode II-shear, Table 2), while vein textures provide information about the velocity of material transfer into the vein with respect to the opening or strain rate (Bons et al., 2000). Along major thrusts, which dominate in the platforms and their boundaries in the MFTB, multiple generations of veins indicate the episodic passage of fluids and fracture filling. These veins were formed from distant source fluids and were probably transported as mobile hydro-fractures (Fisher and Byrne, 1990; Bons, 2001) during thrusting. In contrast, syntectonic veins in the basins typically have sheath shapes, are confined within strata and show dominantly blocky elongate and fibrous textures (Table 2), indicating that the material in the veins is locally derived and that the rate of vein opening (strain) was faster than the transportation of material inside the vein, implying that the most likely mechanism of transport was diffusion (Kirschner et al., 1994; Bons et al., 2000; Oliver and Bons, 2001).

In the platforms it is common to see mm-thick veins (V0) emplaced along stylolitic interfaces, along roughly vertical planes oriented normal to the average stylolite surface. Since stylolites are overall parallel to bedding and are cut by syntectonic cleavage, we assume that they are diagenetic in origin and were roughly horizontal when formed. There is a wide range of estimates of the depth at which stylolites form, based on a variety of approaches, from only 90 m (Tada and Siever, 1989) to 1500–2000 m (Bjørlykke, 1997). In a recent study, based on empirical and theoretical considerations, Ebner et al. (2009) estimate a depth range for formation of 300–600 m. The vertical stress (σv), which, according to Anderson (1976), corresponds to a principal stress, which would have $\sigma 1$ when the stylolites formed. Fig. 8 shows schematically the assumed state of stress for the formation of these extensional veins and stylolites in Mohr circle representation (plot labeled as V0). Fluid pressure must have been sufficiently elevated to allow extensional veins to form, and stress difference small enough, $(\sigma_1 - \sigma_3) < 4t$ (t = tensile strength), that shear failure did not occur. It should be noted that none of the parameters used in constructing Fig. 8 are tightly constrained, but the overall sequence of events and relative magnitudes and orientations of the stresses at different stages are not dependent on closely constraining their values.

V1 veins emplaced parallel to bedding are omnipresent along the cross-section; they can be observed within the thrust slices in

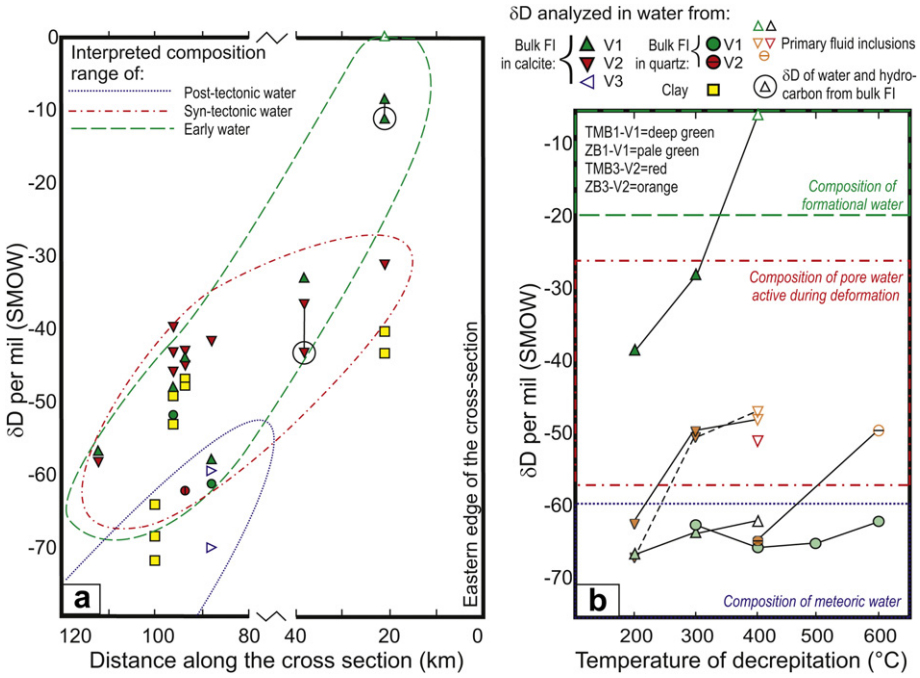

Fig. 7. δD of water in fluid inclusions in veins, and of water in isotopic equilibrium with clays. The V1–V3 veins were collected along the cross-section and the clays from bentonite layers. (a) From water extracted at 400 °C in calcite, 600 °C in quartz, and 1500 ° in clay vs. distance along the cross-section (zero corresponds to the eastern edge, A′ in Fig. 2). δD values correlate with both temperature and intensity of deformation. δD is more negative to the west of the cross-section. (b) δD values measured in water extracted from fluid inclusions within calcite and quartz at 100 °C heating steps (from 200 to 400 °C in calcite and from 200 to 600 °C in quartz), whenever extracted water was available. Note the positive correlation between δD and temperature of extraction.

the platforms and in the basinal carbonate layers. This has important implications for the stress history of the area, because these must have been emplaced at a time when the pore fluid pressures were supra-lithostatic, with the vertical stress (σv) being the smallest principal stress (σ_3), and with a modest stress difference, $(\sigma_1-\sigma_3) < 4t$, which allowed fractures to open against the vertical load and the veins to be emplaced between horizontal strata, prior to folding and thrusting (fig. 8V1). This phenomenon has been commonly observed elsewhere and has been successfully explained in other fold-thrust belts (Jessell et al., 1994; Hilgers et al., 2006). In the study area it likely occurred after tectonic compressional stresses begun to develop, eventually causing the E-W horizontal stress to become the maximum stress. Vein formation parallel to bedding was probably facilitated by the fact that initially tensile strength across bedding planes is smaller than tensile strength for isotropic rock. The emplacement of these veins would have the combined effect of episodically lowering pore fluid pressure and increasing the tensile strength across bedding as the weak contacts between strata sealed following vein emplacement. Increasing tectonic stress would have tended to re-pressurize pore fluids after each failure event. After many bedding-parallel veins had been emplaced, and the difference in tensile strength between bedding normal and isotropic rock had been reduced, conditions were optimum for the production of the V1b veins, which are oblique to bedding and are commonly observed in both basins crosscutting V1a veins (parallel to bedding). These are interpreted as veins filling mixed mode fractures that may develop when $(\sigma_1-\sigma_3)$ is between 4t and 5.6t (Hancock, 1985; Sibson, 1998).

As tectonic compressional stresses increased, the stress difference eventually became large enough, $(\sigma_1-\sigma_3) > 5.6t$, so that the shear strength of the rocks was overcome and thrust faults were produced (fig. 8-V2). The large thrust faults in the platforms formed at this time. At the same time, compressive stresses in the basins produced folds, mostly by ductile deformation, but also with centimeter-scale veins of varying orientations and opening modes (fig. 8-V2). It is likely that tectonic stresses increased slowly and intermittently, with some release after each fracturing or fault-slip event. This is reflected in the crack-seal textures in the syntectonic veins and is consistent with numerical models of the growth of the tectonic wedges that involve episodic slip on faults (e.g. Stockmal et al., 2007). In addition there may be deformation hardening (Kilsdonk and Wiltschko, 1988) that will tend to broaden the deformation in the rock mass. As tectonism ceased, compressive stresses relaxed. In the absence of continued compression, the wedge (see Fitz-Díaz et al., 2011 for a possible reconstruction) became unstable and a gravitational collapse followed, inducing extension (fig. 8-V3). During this stage the maximum stress became vertical again. This explains the formation of extensional veins V3. The stress difference was small enough that tensile failure produced V3 veins in the westernmost platform and basin. In the Zimapán Basin, normal faulting occurred in addition to V3 veining, indicating that stress difference was eventually great enough for shear failure.

5.2. Implications of the $\delta^{18}O$ and $\delta^{13}C$ data

The results of the isotopic analyses in calcite from 'undeformed' limestone in the hanging walls and footwalls of major thrust zones and from associated cataclasites and veins (Fig. 5) can be summarized as follows:

1. Most of the limestones more than a meter away from the thrusts show carbon and oxygen isotopic values typical of Cretaceous carbonates (Weissert et al., 1998; Weissert and Erba, 2004). However, the host rock limestone adjacent to the two westernmost thrusts (Fig. 8, T1 and T5 in the hanging wall and T2 in both hanging wall and footwall) show relatively low $\delta^{13}C$ values.

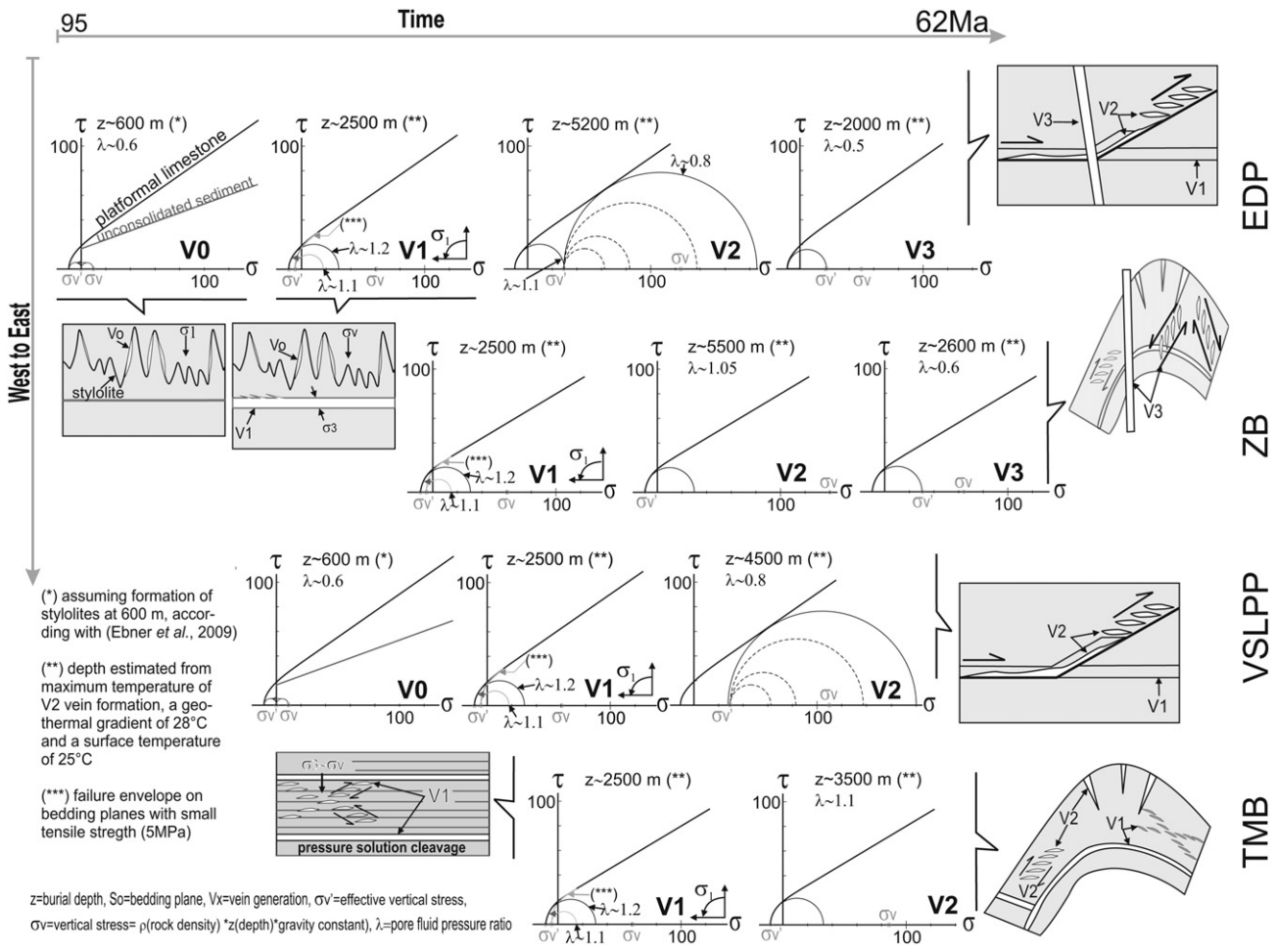

Fig. 8. Inferred and somewhat speculative stress history within the wedge at the stratigraphic level studied, based on relative abundance of vein types (extensional vs. shear) in each generation (V1–V3), burial depth (inferred from temperature of deformation, Fig. 9a), and constraints from theoretical considerations (Griffith, 1921; Byerlee, 1978; Sibson, 1998). Failure mode is assumed to be combined Griffith/Mohr Coulomb (e. g., Price, 1966). Failure envelopes differ for different stages of deformation and limestone types (platformal and basinal). During the emplacement of V0 veins we assumed a poorly consolidated host rock with an angle of internal friction of 20 °, for state of stress we consider that stylolites formed at burial conditions of 600 m (Ebner et al., 2009). During the emplacement of V1, we assumed a tensile strength of 5 MPa along bedding, and angles of internal friction of 35 ° for platformal limestones (as they are dolomitized) and of 30 ° for basinal limestones (Sydney, 1966). During emplacement of V2 and V3 veins, we assumed a tensile strength of 10 MPa along bedding, and angles of internal friction of 35 ° for platformal limestone (dolomitized) and of 30 ° for basinal limestone. Criteria proposed by Sibson (1998) were used in drawing the Mohr circles and for calculating the pore fluid pressure ratios reported, by accounting for estimated burial depths.

2. In cataclasites, the values of $\delta^{13}C$ are lower than those in the veins and host rock for T2, T3, T5 and T6. In the fault zone at T2 the lowest $\delta^{13}C$ values were recorded ($\leq -15‰$) not only in the cataclasites but also in the host El Doctor Platform footwall limestone. This locality is a special case since, even though the contact between the two carbonate units is a thrust, the rocks are in their normal stratigraphic positions (Fig. 2). Along the surface contact there is paleo-karst and paleo-soil development on top of the platform prior to the deposition of syntectonic turbidites above (Hernández-Jáuregui, 1997). To produce such a low $\delta^{13}C$ isotopic exchange with a light carbon source (likely, organic matter) is necessary. Such a source could have been in association with paleo-soils and karsts. There are also low $\delta^{13}C$ values in both the thrust zone and the hanging walls at T1 and to a lesser extent at T5 on the western side of Valles-San Luís Potosí Platform. This feature appears to be accentuated on the hinterland side of the platforms and may be linked to gentle erosion on this side of the platforms, compared to the abrupt propagation fronts of thrust slices on the foreland side, allowing for soil development and infiltration of meteoric fluids.

The $\delta^{13}C$ anomalies in most of the cataclasites in the thrusts bounding the Zimapán and Tampico-Misantla Basins on their western sides (T3 and T6) are probably caused by the presence of hydrocarbons, or due to mobilization of ^{13}C-rich calcite by pressure-solution. Western thrusts are longer lived than their eastern counterparts; therefore such anomalies may reflect a longer thrusting history, organic matter maturation and escape along the thrusts. Hydrocarbons were likely locally derived, as the carbonate sequences in the area, especially basinal limestones, are rich in organic matter (Valencia-Islas, 1996). The low $\delta^{13}C$ values observed in the thrust zones on the western edges of the Zimapán and Tampico-Misantla basins (Figs. 2 and 5, T6 and T3) suggest that hydrocarbon transformation is controlled by the deformation paths within the wedge. This is expected because the deformation determines the thickening within the wedge, and therefore burial conditions.

3. The largest shifts in $\delta^{18}O$ occur in calcite megacrystals from late veins, observed only in the two westernmost thrusts (T1 and T2); $\delta^{18}O$ shifts (with respect to the host rock) are more accentuated in calcite veins than in cataclasites. In other thrusts

$\delta^{18}O$ is the same in veins, cataclasites, and host rocks (Fig. 5, T1 and T2). $\delta^{18}O$ shifts in calcite from veins in the fault zones were probably caused by meteoric, water provided that the veins show no anomalies in $\delta^{13}C$. Meteoric fluids probably infiltrated the westernmost part of the cross-section and were channeled along major faults. There is less carbonate in the rocks on the western edge of the cross-section to provide isotopic buffering. The absence of significant $\delta^{18}O$ shifts in the other thrusts (T3–T7) suggests that (1) the fluid circulating through them was compositionally close to that of the carbonate host rocks, (2) they were volumetrically limited, or (3) there was enough time under appropriate temperature conditions for isotopic buffering to occur (Kirschner and Kennedy, 2001).

The $\delta^{13}C$ and $\delta^{18}O$ values in V1 and V2 veins (fold and shear-related veins developed in thrust slices) are very close to those in the enclosing host rocks (except for locality VP1), and are different from those of most of the V3 veins. $\delta^{13}C$ and $\delta^{18}O$ from V1 and V2 veins from locality VP1 are roughly distributed along a line with a positive slope that could represent a 'mixing line' (Phillips et al., 2005) between a fluid poor in heavy carbon and oxygen and host rocks (Fig. 6).

Since deformation occurred between 90 and 65 Ma, based on stratigraphic constraints (Fitz-Díaz et al., in press), the overall rate of deformation, which is linked to the dissolution-precipitation rate, appears to have been slower than the rate of isotopic exchange between calcite and water (Cole, 2000; Chacko et al., 2001). V1 veins are assumed to have formed at about the same temperature (roughly 70 °–100 °C) as elsewhere, while V2 veins formed at 100 °–250 °C (Fig. 9a), according to temperature determinations from fluid inclusion, illite crystallinity, and vitrinite analyses (Valencia-Islas, 1996; Gray et al., 2001; Fitz-Díaz et al., 2011; Ortega Flores, 2011). V3 veins formed 70 °–160 °C (Muñoz-Máximo, 2011, Fig. 9a). The isotopic composition of calcite of V2 veins and host rocks is similar. This has two possible explanations: 1) there was a large amount of fluid in the reservoir with a similar composition to the host rock; 2) there was a restricted amount of pore fluid with an initially different composition that was buffered by the host rock during deformation. We know that temperature varies along the cross-section (from 100 to 300 °C). V3 veins in DP1 and ZB4, and V1 and V2 veins in VP1 are likely to have been affected by fluids with low $\delta^{13}C$ and $\delta^{18}O$ values, probably meteoric. It seems likely such fluids inflowed during the late extensional phase in the western part of the study area, including the El Doctor Platform and the Zimapán Basin. The data also suggest that the Valles-San Luis Potosí Platform behaved as an open system during the shortening stage of deformation. Alternatively, calcite veins were initially buffered by the host rock and later recrystallized or reprecipitated during deformation while exposed to external fluids. This could be due to brittle deformation allowing the inflow of low-temperature meteoric fluids (~160 °C, Fig. 9a; Valencia-Islas, 1996; Gray et al., 2001). The influence of meteoric water is reflected in the 'mixing line' trend (Fig. 5VP1). Although rocks of the adjacent Tampico-Misantla Basin were shortened under lower temperatures (90 °–190 °C) than the rocks of the Valles-SLP Platform, the fact that the isotopic compositions of vein calcite and host rocks in the basin are similar suggests that temperature was not the main factor controlling isotopic exchange. The influence of meteoric fluids must have been limited in the basin, which behaved as a quasi-closed system for fluids during deformation. The fluids in the basin rocks would likely have been formational water or brines, which is compatible with evidence from fluid inclusion analysis in other parts of the MFTB (Fischer et al., 2009; González-Sánchez et al., 2009).

5.3. δD and sources for fluids during deformation

Unlike the $\delta^{18}O$ values in the veins, most of which have been buffered by the host rock due to intense fluid–rock interaction, δD from fluid inclusions and illite/smectite preserves better the original signature of aqueous fluids. δD in fluid inclusions from V1 and V2 veins decreases westwards, a feature that may be the result of the increasing interaction between original pore water and meteoric water, which probably infiltrated through the abrupt topography at the back of the wedge. V3 veins show the lowest δD values (−70 to −60‰) and, as part of a network of sub-vertical extensional veins, the fractures they fill could have provided pathways for the inflow of meteoric fluids. The values of c δD in the V3 veins are

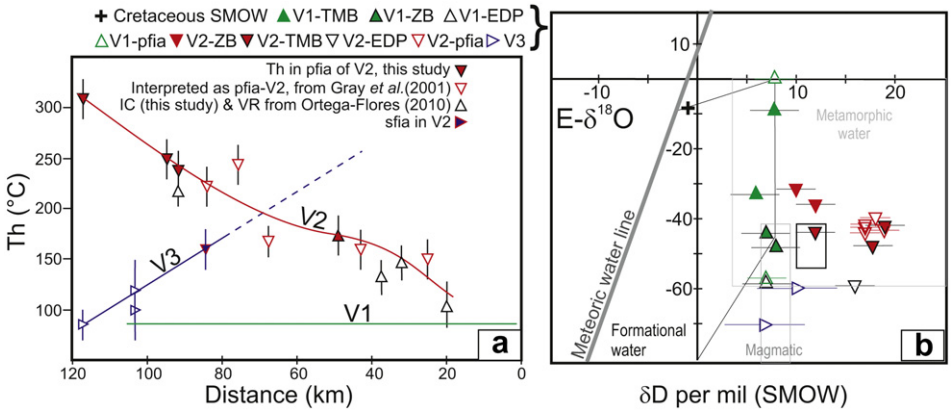

Fig. 9. Temperature of deformation and isotopic composition of water from fluid inclusions. (a) Temperature profile for V1–V3 during deformation, based on a compilation of microthermometry of fluid inclusions reported in the area from this work (in solid symbols) and works by Valencia-Islas (1996); Gray et al. (2001); Muñoz-Máximo (2011), in open symbols. The temperature ranges are in accordance with other thermometric methods (illite crystallinity, vitrinite reflectance, thermochronology) applied in the area. (b) $\delta^{18}O$ vs. δD plot for water from different vein generations and comparison with the meteoric water line and other possible sources of water. The range of $\delta^{18}O$ in fluid inclusions was calculated from $\delta^{18}O_{calcite}$, by assuming equilibrium and applying the ranges of temperature of deformation (as for plot a), and equilibrium-state equations of O'Neil et al., (1969) and Zheng (1994). The meteoric water line is based on measurements of recent meteoric water in Mexico (Wassenaar et al., 2009), which does not significantly differ from the Craig (1961) meteoric water line. The envelopes for formational and magmatic waters were taken from Taylor (1974). The SMOW composition for Cretaceous times comes from (Eslinger and Yeh, 1986). Open symbols correspond to fluid inclusions released at the highest temperatures during decrepitation, presumably primary (green for V1, red for V2 veins and blue for V3 veins). IC = illite crystallinity, VR = Vitrinite Reflectance, pfia = primary fluid inclusion association, sfia = secondary fluid inclusion association. (For interpretation of the references to color in this figure legend, the reader is referred to the web version of this article.)

similar to those of recent meteoric water in Mexico (Wassenaar et al., 2009), although δD for Cretaceous meteoric water could have been lower than present values due to higher average annual temperatures at that time.

The systematic change in the values of δD of water released during heating steps implies that primary inclusion fluids were trapped at higher temperatures and have higher δD values than secondary inclusions. The exception is a V1 vein from ZB1 for which all steps yielded low δD values (Fig. 7b). It is suggested that δD values (−11–0‰, Appendix 2) from fluid inclusion water in V1 in the easternmost localities is perhaps closest to the original composition of formational water, as they are the closest to SMOW. In the same localities, a calculated value of δD ∼−15‰ was obtained for water in isotopic equilibrium with the clay minerals at 80 °C during diagenesis and V1 emplacement, following equations of Yeh (1980) and Hyeong and Capuano (2004). This value is also close to both present and Cretaceous SMOW (Fig. 9b). Similar cases tracking changes in δD during diagenesis and deformation/uplift have been reported by Compton et al. (1999) and Eslinger and Yeh (1986).

There is no evidence for the presence of metamorphic or magmatic fluids during deformation. The deformation occurred at very low metamorphic grade and the Grenville gneiss basement appears to have been only affected by brittle shear along the detachment zone, with no associated metamorphism (Suter, 1984; Ochoa-Camarillo, 1996). Only clay dehydration (smectite to illite) in deformed bentonite layers (interbedded with basinal limestones) occurred. Such a reaction is in accordance with temperature constraints (Fig. 9a).

The presence of diagenetic stylolites indicates that the Cretaceous carbonates were buried to a depth of around 600 m (Ebner et al., 2009), where the porosity of the rock would be 10–20% of the total volume (e. g.,Schmoker and Gautier, 1989) or less, as cementation might have sealed a considerable amount of the pore volume (Bjørlykke, 1997). During this process expandable clays could have taken up seawater. Compaction of shaly layers would likely have decreased permeability due to the alignment and growth of platy-shaped clays, thus elevating the pore and clay fluid confinement within the layers. During the formation of V1 such water was the likeliest vehicle for dissolution-precipitation, and some would have been trapped in primary fluid inclusions. Part of this seawater would have been expelled from the basin as deformation progressed and rock porosity was further reduced. Based on the obtained temperatures of deformation, a reasonable estimate of the maximum burial depth at the front of the cross-section (assuming a surface T of 25 °C and a geothermal gradient of 28 °C/km) is 3–4 km, in which case porosity would have been reduced to ∼10% (e.g.,Schmoker and Gautier, 1989). Thus pore fluids, essentially formational water, at the peak of the deformation were probably <10% of the total volume. Then, if formational water was the total budget available to produce V2 veins (Fig. 3b–d), it had to be re used during deformation and/or supplemented by adding meteoric fluids, since, according to experimental observations, the water/calcite volume ratio needed to precipitate veins is far larger (10^5–10^6, Lee and Morse, 1999) than the reservoir (rock porosity)/host rock volume ratio of the deformed rocks.

6. Discussion

The basic concepts connecting processes and fluid reservoirs and linking the mechanics of deformation to fluid flow within the MFTB are illustrated in Fig. 10, This leads to a schematic visualization of the integrated evolutionary model presented in Fig. 11. The model integrates structural, isotopic and fluid inclusion data, to account for temperature (T), effective pressure, clay dehydration reactions, and fluid–rock interaction during the progressive growth of the fold-thrust belt. Note that this strictly applies only to the stratigraphic interval studied. Based on field observations, we believe this is representative of the entire package of Cretaceous sedimentary strata that constitute the fold-thrust belt wedge, although the pattern would likely require some modification if the detailed analysis were to be extended to all stratigraphic levels. The model starts with the formation of V1 veins (Fig. 11a) in the El Doctor Platform and ZB. These formed when compressive tectonic stresses first built up, causing σ1 to switch from vertical to horizontal, but at a time when σh did not differ much from σv. The tectonic stress would have enhanced the pore fluid pressure, which must have exceeded the lithostatic load (σv, fig. 8-V1) for the veins to have formed. $\delta^{13}C$ and $\delta^{18}O$ in vein calcite are buffered by the host limestones. At this stage, most of the rock volume would have been under the sea; therefore the fluids (volumetrically restricted to primary porosity) active during deformation would have been formational waters with a δD close to SMOW.

In a second stage (Fig. 11b), shortening by thrusting and folding on the western side of the cross-section created vertical thickening in EDP and ZB. Such thickening led to an increase in temperature on the western side of the cross-section, following the regional geothermal gradient. Thickening also resulted in emergence of the rocks above sea level. Once exposed to atmospheric conditions, the rocks interacted with meteoric fluids. Since the EDP included few impervious clay horizons and experienced mostly brittle deformation, the faults and fracture network that developed in it probably allowed meteoric fluids to percolate. Such fluids would have interacted to some extent with the rock within the thrust slices, thus bringing low δD water into the primary fluid inclusions in V2 veins and secondary inclusions in V1. Some meteoric water likely reached deeper levels in the growing wedge and finally interacted with foreland rocks, thus decreasing the overall δD in pore water.

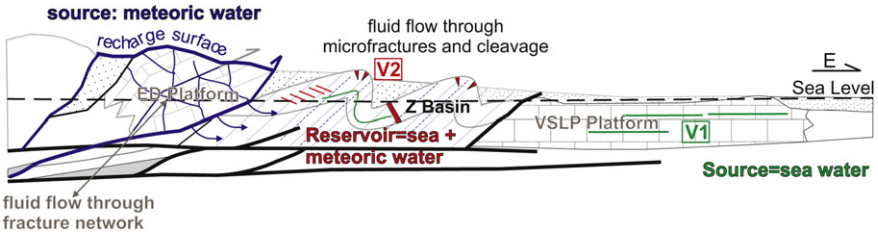

Fig. 10. Basic concepts relating deformation to fluid flow in the MFTB wedge. This model shows a thin-skinned orogenic wedge, with higher topography to the west that allowed the carbonates to emerge from the sea level. Two possible sources of water active during deformation are assumed, meteoric and formational water. Formational water is more abundant to the front of the wedge, while the influence of meteoric water is more important to the back of the wedge and in the platforms, where the fracture network allows a more efficient percolation. Fluid flow within the basins possibly occurred along micro-fractures and cleavage planes; water-rock interaction was probably more important in the basins than in the platforms.

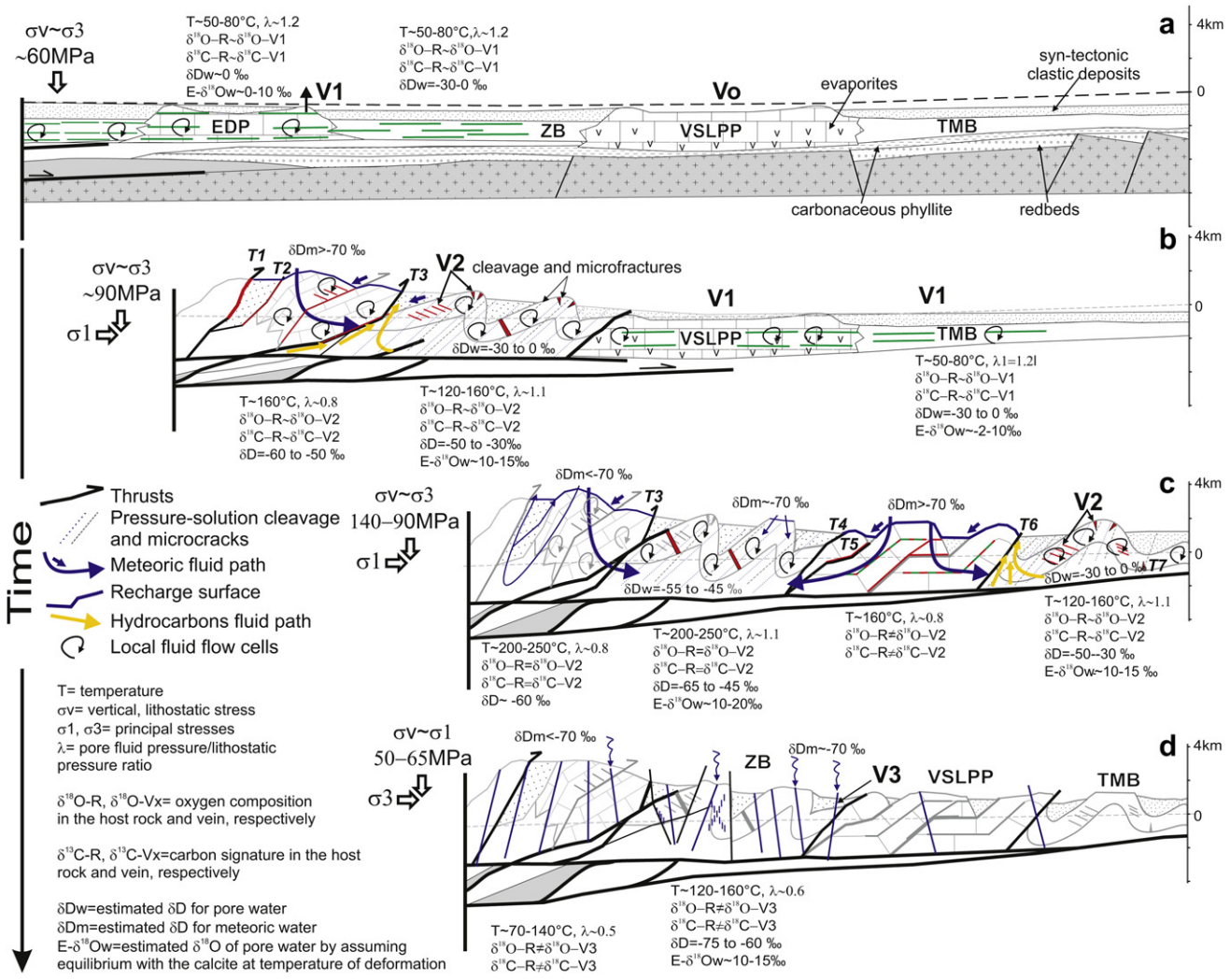

Fig. 11. Conceptual model scenarios for the tectonic evolution of the MFTB. Each stage (a–d) shows the possible temperature of deformation, state of stress, pore fluid pressure, and isotopic signature of aqueous fluids during deformation at different locations within the wedge. It also includes possible paths for aqueous fluids (blue) and hydrocarbons during deformation (yellow). (For interpretation of the references to color in this figure legend, the reader is referred to the web version of this article.)

Basinal limestones interbedded with impervious shales prevented meteoric fluid penetration and contributed to enhanced pore fluid pressure to supra-lithostatic conditions. The V2 veins in the ZB were emplaced under these conditions. However, in the platform the major thrusts and probably part of the fracture network would still have been connected to the surface, which would have kept the pore fluid pressure to infra-lithostatic conditions.

In a third stage, as the wedge grew eastwards, the Valles-SLP Platform and the Tampico-Misantla Basin would have experienced similar conditions to those in the El Doctor Platform and Zimapán Basin during the previous stage. Meanwhile the El Doctor Platform and Zimapán Basin continued to shorten and thicken (Fig. 11c). At this stage, the tectonic stresses probably peaked, since the wedge then reached its maximum thickness, deepest burial conditions, and therefore also maximum T of deformation at the base and at the rear of the wedge (figs. 8-V2 and 9a-V2). Extensional V2 veins confined to layers were still developing in the ZB, suggesting that the pore fluid pressure was still, at least intermittently, supra-lithostatic. By contrast, in the platforms, and especially the Valles-SLP Platform, the values of $\delta^{13}C$ and $\delta^{18}O$ in V2 veins are lower than those in the host rocks, indicating the presence of meteoric water and limited fluid–rock interaction (T of deformation in the Valles-SLP Platform was ~160 °C). The $\delta^{18}O$ and $\delta^{13}C$ values in V1 in the Valles-SLP Platform also differ from those in host rocks, indicating that V1 calcite probably recrystallized or was reprecipitated during deformation. In the Tampico-Misantla Basin, in contrast, $\delta^{18}O$ and $\delta^{13}C$ in V1 and V2 are buffered by host rocks, even though the T of deformation was lower there than in the Valles-SLP Platform. This is probably because of the confining fluid conditions within the basin, making the rocks and veins developed there less susceptible to the influence of meteoric fluids than the platform nearby.

Field evidence and microthermometric data indicate that V3 veins on the western side of the study area were emplaced at lower temperatures than V2 veins. The isotopic composition of the V3 veins was not completely buffered by the host rock, but rather was the result of interaction between isotopically lighter fluids, probably meteoric, and the host limestones. The *en-échelon* distribution of some V3 vein arrays indicates conditions of higher confining pressure in the Zimapán Basin than in the El Doctor Platform. In the latter sub-vertical veins up to a few hundred meters long suggest more open and connected pathways to the surface. Further evidence for such a difference in conditions between basin and platform is that V3 veins in some localities in the Zimapán Basin are

isotopically buffered by host rocks, whereas in the El Doctor Platform they are not. Also, temperatures of homogenization in V3 are higher in the Zimapán Basin than in the El Doctor Platform, so it is interpreted that V3 veins formed deeper in the Zimapán Basin than in the El Doctor Platform. δD values in V3 support the idea of meteoric water influence (Fig. 11d).

Mesoscopic structural observations indicate that most of the V1 and V2 veins in the basins formed under confining conditions during tectonic shortening. However, the δD signatures indicate a progressively greater influence of meteoric fluids with time (Fig. 10). The $\delta^{13}C$ and $\delta^{18}O$ signatures of veins were probably buffered without much change in δD because the volume of formational fluids was limited. These fluids upwelled into basinal carbonates through microcracks and cleavage surfaces. Infiltration of meteoric fluids would have been possible along bedding planes after the erosion of folded layers (Fig. 11c).

7. Conclusions

The structural and kinematic analysis of mesoscopic shortening structures at a regional scale, together with stratigraphic constraints, provide insight into progressive deformation and the role of fluids during deformation within the Mexican Fold and Thrust Belt. Lateral facies variations of carbonate sequences played a major role in controlling deformation styles: thrusting was dominant in the massive carbonate platforms and folding dominant in basinal sequences. Major thrusts within and at the borders of platforms, together with associated fracture networks were efficient pathways for fluids. Fluid pathways in the basinal carbonate facies are not so obvious because fold-related veins were emplaced between and within limestone layers, interstratified with shales and bentonites. Nevertheless, isotopic studies point to the presence and influence of meteoric fluids during deformation to varying degrees.

The analysis of δD in water from fluid inclusions in veins emplaced early, during and after the main deformation event (V1–V3, respectively) in different positions along the studied cross-section, indicates a progressively greater influence of meteoric fluids with time and distance from the toe of the wedge. Values of δD in illite/smectite in the basinal rocks show a similar trend and range of values, additionally suggesting that meteoric fluids interacted with clays during deformation as smectite transformed into illite. Since fluid pathways for meteoric water are not conspicuous at a mesoscopic scale in the basinal carbonates, it is likely that fluids moved through microcracks and associated with solution transfer.

$\delta^{13}C$ and $\delta^{18}O$ isotopic compositions of veins and basinal limestones indicate an intense interaction between pore fluids and host rocks, early and during deformation and under different strain conditions, at 90 °–300 °C. This interaction caused isotopic buffering of the veins. However, the buffering was not effective in some localities of the Valles-SLP Platform, probably due to the extensive influence of meteoric fluids. $\delta^{13}C$ and $\delta^{18}O$ along transects of major thrusts provide evidence for the passage of meteoric water along the two westernmost thrusts, and for the occurrence of hydrocarbons on the western boundaries of the basins. The latter suggests an asymmetric flow of hydrocarbons, which would have been influenced by the flow of rocks during deformation. In other words, the flow of hydrocarbons was extensively controlled by the orogenesis.

There is a very good correlation among the horizontal gradient and temperature of deformation, the influence of meteoric fluids, and clay dehydration reactions along the stratigraphic interval in which attention was focused in the studied cross-section. This is consistent with critical taper orogenic wedge theory, which predicts that deformation starts at the back end of the wedge (the western side of the cross-section), and progresses toward the foreland, thus thickening and incorporating more strata as the wedge grows, producing deepening burial conditions and thus higher temperatures of deformation. Subsequently, faster exhumation occurred at the rear of the wedge. This scenario provides a longer time for the rocks on the western side of the cross-section to be exposed to meteoric water.

Acknowledgments

This paper is part of the PhD dissertation at the University of Minnesota of the first author, who thanks CONACyT for sponsoring the first three years of her doctoral study. We thank the Universidad Nacional Autónoma de México (PAPIIT grant 1210063), and the University of Minnesota for financial support in carrying out this research. We also thank Saint Louis University and the Université de Lausanne for allowing us to use their facilities for stable isotope analysis, which was essential for this project. We thank Torsten Vennemann for his useful suggestions and insight during lab work at Lausanne. We acknowledge the help provided by Jaime Díaz Ortega during clay separation. Finally, we thank Kieran O'Hara and David Wiltschko for their most helpful reviews.

Appendix. Supplementary material

Supplementary data associated with this article can be found, in the online version, at doi:10.1016/j.jsg.2011.05.009.

References

Abdioglu, E., Arslan, M., 2005. Mineralogy, geochemistry, and genesis of bentonites of the Ordu Area, NE Turkey. Clays and Clay Minerals 40, 131–151.
Anderson, E.M., 1976. The dynamics of faulting. In: Voight, B., Fairbridge, R.W. (Eds.), Mechanics of Thrust Faults and Decollement. Dowden, Hutchinson, Ross, Stroudsburg, PA, United States (USA).
Armstrong, R.L., 1974. Magmatism, orogenic timing, and orogenic diachronism in the cordillera from Mexico to Canada. Nature (London) 247, 348–351.
Bjørlykke, K., 1997. Lithological control on fluid flow in sedimentary basins. In: Jamtveit, B., Yardley, B. (Eds.), Fluid Flow and Transport in Rocks: Mechanisms and Effects. Chapman and Hall, Oxford, U.K, pp. 15–34.
Bjørlykke, K., Ramm, M., Saigal, G.C., 1989. Sandstone diagenesis and porosity modification during basin evolution; geologic modeling; aspects of integrated basin analysis and numerical simulation. Geologische Rundschau 78, 243–268.
Bodnar, R.J., Vityk, M.O., 1994. Interpretation of microthermometric data for H_2O–NaCl fluid inclusions. In: De Vivo, B., Frezzotti, M.L. (Eds.), Fluid Inclusions in Minerals, Methods and Applications. Virginia Tech, Blacksburg, VA, pp. 117–130.
Bons, P.D., 2001. The formation of large quartz veins by rapid ascent of fluids in mobile hydrofractures; fluids and fractures in the lithosphere. Tectonophysics 336, 1–17.
Bons, P.D., Jessell, M.W., Urai, J.L., 2000. The formation of veins and their microstructures; Stress, strain and structure; a volume in honor of W. D. Means. Journal of the Virtual Explorer 2.
Burkhard, M., 1993. Calcite twins, their geometry, appearance and significance as stress-strain markers and indicators of tectonic regime; a review; the geometry of naturally deformed rocks. Journal of Structural Geology 15, 351–368.
Byerlee, J.D., 1978. Friction of rocks; rock friction and earthquake prediction. Pure and Applied Geophysics 116, 615–626.
Byerlee, J.D., 1993. A model for episodic flow of high pressure water in fault zones before earthquakes. Geology 21, 303–306.
Campa-Uranga, M.F., 1983. Geological Sciences. The Tectonostratigraphic Terranes and the Thrust Belt in Mexican Territory; Proceedings of the Circum-Pacific Terrane Conference, 18. Stanford University Publications. 44–46.
Carrillo-Martínez, M., 1989. Structural analysis of two juxtaposed Jurassic lithostratigraphic assemblages in the Sierra Madre Oriental fold and thrust belt of central Mexico: dynamics and evolution of the lithosphere. Geofísica Internacional 28, 1007–1028.
Carrillo-Martínez, M., 1990. Geometría estructural de la Sierra Madre Oriental entre Peñamiller y Jalpan, Estado de Querétaro. Revista del Instituto de Geología 8, 62–70.
Carrillo-Martínez, M., Valencia-Islas, J.J., Vázquez, M.E., 2001. Geology of the southwestern sierra madre oriental fold-and-thrust belt, east-central Mexico: a review. AAPG Memoir 75, 145–158.
Chacko, T., Cole, D.R., Horita, J., 2001. Equilibrium oxygen, hydrogen and carbon isotope fractionation factors applicable to geologic systems: stable isotope geochemistry. Reviews in Mineralogy and Geochemistry 43, 1–81.

Cole, D.R., 2000. Isotopic exchange in mineral-fluid systems. IV. The crystal chemical controls on oxygen isotope exchange rates in carbonate-H_2O and layer silicate-H_2O systems. Geochemica et Cosmochemica Acta 65–5, 921–931.
Compton, J.S., Conrad, M.E., Vennemann, T.W., 1999. Stable isotope evolution of volcanic ash layers during diagenesis of the Miocene Monterey Formation, California. Clays and Clay Minerals 47, 84–95.
Coney, J., Evenchick, C.A., 1994. Consolidation of the American Cordilleras. Journal of South American Earth Sciences 7, 241–262.
Coney, P.J., Jones, D.L., Monger, J.W.H., 1980. Cordilleran suspect terranes. Nature (London) 288, 329–333.
Cox, S.F., 2007. Structural and isotopic constraints on fluid flow regimes and fluid pathways during upper crustal deformation; an example from the Taemas area of the Lachlan Orogen, SE Australia. Journal of Geophysical Research 112 @B08208.
Cox, S.F., Etheridge, M.A., Wall, V.J., 1987. The role of fluids in syntectonic mass transport, and the localization of metamorphic vein-type ore deposits. Ore Geology Reviews 2, 65–86.
Craig, H., 1961. Isotopic variations in meteoric waters. Science 133, 1702–1703.
Crispini, L., Frezzotti, M.L., 1998. Fluid inclusion evidence for progressive folding during decompression in metasediments of the Voltri Group (Western Alps, Italy). Journal of Structural Geology 20, 1733–1746.
Dahlen, F.A., 1990. Critical taper model of fold-and-thrust belts and accretionary wedges. Annual Review of Earth and Planetary Sciences 18, 55–99.
Dahlen, F.A., Suppe, J., Davis, D., 1984. Mechanics of fold-and-thrust belts and accretionary wedges; cohesive Coulomb theory, Special section: S. Thomas Crough memorial. Journal of Geophysical Research 89, 10,087–10,101.
Davis, D., Suppe, J., Dahlen, F.A., 1983. Mechanics of fold-and-thrust belts and accretionary wedges. Journal of Geophysical Research 88, 1153–1172.
DeCelles, P.G., 2004. Late jurassic to eocene evolution of the cordilleran thrust belt and foreland basin system, western U.S.A. American Journal of Science 304, 105–168.
Durney, D.W., 1972. Solution-transfer, an important geological deformation mechanism. Nature (London) 235, 315–317.
Ebner, M., Koehn, D., Toussaint, R., Renard, F., Schmittbuhl, J., 2009. Stress sensitivity of stylolite morphology. Earth and Planetary Science Letters 277, 394–398.
Engelder, T., 1984. The role of pore water circulation during the deformation of foreland fold and thrust belts. Journal of Geophysical Research 89, 4319–4325.
Eslinger, E.V., Yeh, H., 1986. Oxygen and hydrogen isotope geochemistry of cretaceous bentonites and shales from the disturbed belt, Montana. Geochimica et Cosmochimica Acta 50, 59–68.
Evenchick, C.A., McMechan, M.E., McNicoll, V.J., Carr, S.D., 2007. A synthesis of the Jurassic-Cretaceous tectonic evolution of the central and southeastern Canadian Cordillera; exploring links across the orogen; Whence the mountains? Inquiries into the evolution of orogenic systems; a volume in honor of Raymond A. Price. Special Paper – Geological Society of America. 433, 117–145.
Ferket, H., Swennen, R.A.J., Ortuño, S., Roure, F., 2003. Reconstruction of the fluid flow history during Laramide foreland fold and thrust belt development in eastern Mexico; cathodoluminescence and $\delta^{18}O$–$\delta^{13}C$ isotope trends of calcite-cemented fractures. Journal of Geochemical Exploration 78–79, 163–167.
Fischer, M.P., Higuera-Diaz, I.C., Evans, M.A., Perry, E.C., Lefticariu, L., 2009. Fracture-controlled paleohydrology in a map-scale detachment fold; insights from the analysis of fluid inclusions in calcite and quartz veins. Journal of Structural Geology 31, 1490–1510.
Fisher, D.M., Brantley, S.L., 1992. Models of quartz overgrowth and vein formation; deformation and episodic fluid flow in an ancient subduction zone. Journal of Geophysical Research 97, 20,043–20,061.
Fisher, D.M., Byrne, T., 1990. The character and distribution of mineralized fractures in the Kodiak Formation, Alaska; implications for fluid flow in an underthrust sequence; Special section on the Role of fluids in sediment accretion, deformation, diagenesis, and metamorphism in subduction zones. Journal of Geophysical Research 95, 9069–9080.
Fitz-Díaz, E., Tolson, G., Hudleston, P., Bolaños-Rodríguez, D., Ortega-Flores, B., Serrano-Vázquez, A., in press. The role of folding in the development of the Mexican fold-thrust belt, in: Cerca M., Chávez-Cabello, G., Valencia, M. The Laramide Orogeny in Mexico. Geological Society of America Special Paper, (in press).
Fitz-Díaz, E., Hudleston, Tolson, G., 2011. Comparison of tectonic styles in the Mexican and Canadian Rocky mountain fold-thrust belt. In: Poblet, J., Lisle, R. (Eds.), Kinematics and Tectonic Styles of Fold-Thrust Belt, Geological Society of London, 349. Special Publication, pp. 149–167.
Foreman, J.L., Dunne, W.M., 1991. Conditions of vein formation in the Southern Appalachian foreland; constraints from vein geometries and fluid inclusions. Journal of Structural Geology 13, 1173–1183.
Fyfe, W.S., Kerrich, R., 1985. Fluids and thrusting. Chemical Geology 49, 353–362.
Goldstein, R.H., Reynolds, T.J., 1994. Systematics of fluid inclusions in diagenetic minerals. SEPM Short Course Notes 31, 199.
González-Sánchez, F., Camprubí, A., González-Partida, E., Puente-Solís, R., Canet, C., Centeno-García, E., Atudorei, V., 2009. Regional stratigraphy and distribution of epigenetic stratabound celestine, fluorite, barite and Pb–Zn deposits in the MVT province of northeastern Mexico. Miner Deposita 44, 343–361.
Grant, N.T., Banks, D.A., McCaig, A.M., Yardley, B.W.D., 1990. Chemistry, source, and behavior of fluids involved in Alpine thrusting of the central Pyrenees; Special section on the Role of fluids in sediment accretion, deformation, diagenesis, and metamorphism in subduction zones. Journal of Geophysical Research 95, 9123–9131.
Gray, G.G., Pottorf, R.J., Yurewicz, D.A., Mahon, K.I., Pevear, D.R., Chuchla, R.J., 2001. Thermal and chronological record of syn-to post-Laramide burial and exhumation, Sierra Madre Oriental, Mexico; The western Gulf of Mexico basin; tectonics, sedimentary basins, and petroleum systems. AAPG Memoir 75, 159–181.
Griffith, A.A., 1921. The phenomena of rupture and flow in solids. Philosophical Transactions of the Royal Society of London A 221, 163–198.
Hancock, P.L., 1985. Brittle microtectonics: principles and practice. Journal of Structural Geology 7, 437–457.
Hernández-Jáuregui, R. 1997. Sedimentación sintectónica de la Formación Soyatal (Turoniano Medio-Campaniano) y modelado cinemático de la cuenca de flexura de Maconí, QuerétaroInstituto Politécnico Nacional, ESIA, (Masters Thesis).
Hilgers, C., Kirschner, D.L., Breton, J.P., Urai, J.L., 2006. Fracture sealing and fluid overpressures in limestones of the Jabal Akhdar Dome, Oman mountains. Geofluids 6, 168–184.
Hodgkins, M.A., Stewart, K.G., 1994. The use of fluid inclusions to constrain fault zone pressure, temperature and kinematic history; an example from the Alpi Apuane, Italy. Journal of Structural Geology 16, 85–96.
Hubbert, M.K., Rubey, W.W., 1959. Mechanics of fluid-filled porous solids and its application to overthrust faulting, Part 1 of Role of fluid pressure in mechanics of overthrust faulting. Geological Society of America Bulletin 70, 115–166.
Hyeong, K., Capuano, R.M., 2004. Hydrogen isotope fractionation factor for mixed-layer illite/smectite at 60 degrees to 150 degrees C; new data from the northeast Texas Gulf Coast. Geochimica et Cosmochimica Acta 68, 1529–1543.
Imlay, R.W., 1944. Correlation of the Cretaceous formations of the greater Antilles, central America and Mexico Chart no. 10-A. Geological Society of America Bulletin 55, 1005–1045.
Jessell, M.W., Willman, C.E., Gray, D.R., 1994. Bedding parallel veins and their relationship to folding. Journal of Structural Geology 16, 753–767.
Kilsdonk, B., Wiltschko, D.V., 1988. Deformation mechanisms in the southeastern ramp region of the Pine mountain Block, Tennessee; with Suppl. Data 88-12. Geological Society of America Bulletin 100, 653–664.
Kirschner, D.L., Kennedy, L.A., 2001. Limited syntectonic fluid flow in carbonate-hosted thrust faults of the Front Ranges, Canadian Rockies, inferred from stable isotope data and structures. Journal of Geophysical Research 106, 8827–8840.
Kirschner, D.L., Sharp, Z.D., Teyssier, C., 1993. Vein growth mechanisms and fluid sources revealed by oxygen isotope laser microprobe. Geology (Boulder) 21, 85–88.
Kisch, H.J., 1990. Calibration of the anchizone; a critical comparison of illite "crystallinity" scales used for definition. Journal of Metamorphic Geology 8, 31–46.
Kübler, B., 1967. La cristallinité de l'illite et les zones tout à fait supérieures du metamorphisme. Étages tectoniques. Colloque de Neuchâtel, 18–21. avril 1966. Université de Neuchâtel, Institut de Géologie, 105-122.
Kübler, B., 1968. Évaluation quantitative du métamorphisme par la cristallinité de l'illite; état des progrès realisés ces dernières années. Centre de Recherches de Pau (Societé Nationale des Petôles d'Aquitaine). Bulletin 2, 385–397.
Kübler, B., Jaboyedoff, M., 2000. Illite crystallinity. Comptes Rendus de l'Académie des Sciences. Série II.Sciences de la Terre et des Planètes 331, 75–89.
Lee, Y.J., Morse, J.W., 1999. Calcite precipitation in synthetic veins: implications for the time and fluid-volume necessary for vein filling. Chemical Geology 156, 151–170.
López-Ramos, E., 1983. Estratigrafia Cretacica y tectonica de una porcion del centro y noreste de Mexico. Cretaceous stratigraphy and tectonics of a portion of the central and northeast of Mexico. Boletín de la Sociedad Geológica Mexicana 44, 21–31.
Moore, D.M., Reynolds Jr., R.C., 1997. X-ray Diffraction and the Identification and Analysis of Clay Minerals. Oxford University Press, Oxford, United Kingdom, 373 pp.
Moore, J.C., Vrolijk, P., 1992. Fluids in accretionary prisms. Reviews of Geophysics 30, 113–135.
Moore, J.C., Brown, K.M., Horath, F., Cochrane, G.R., MacKay, M., Moore, G., 1991. Plumbing accretionary prisms; effects of permeability variations. Philosophical Transactions of the Royal Society of London, Series A: Mathematical and Physical Science 335, 275–288.
Muñoz-Máximo, I. 2011. esAnálisis de inclusiones fluidas e isótopos estables en mega-vetas de calcita y su significado estructural en el área de Zimapán y Peñamiller, Estados de Hidalgo y Querétaro. Bachelor's thesis, Benemérita Universidad Autónoma de Puebla. 150 pp.
Ochoa-Camarillo, H. 1996. Geología del anticlinorio de Huayacocotla en la región de Molango, Estado de Hidalgo. Instituto de Geología, UNAM, Master's thesis, 91 pp.
Oliver, N.H., Bons, P., 2001. Mechanisms of fluid flow and fluid–rock interaction in fossil metamorphic hydrothermal systems inferred from vein–wallrock patterns, geometry and microstructure. Geofluids 1, 137–162.
O'Neil, J.R., Clayton, R.N., Mayeda, T.K., 1969. Oxygen isotope fractionation in divalent metal carbonates. The Journal of Chemical Physics 51, 5547–5558.
Ortega-Flores, B. 2011. Deformación por acortamiento en la Plataforma Valles-San Luís Potosí y en la Cuenca Tampico-Misantla; porción externa del Cinturón de Pliegues y Cabalgaduras Mexicano. Master's Thesis, Programa de Posgrado en Ciencias de la Tierra, Universidad Nacional Autónoma de México, 104 pp.
Phillips, D.L., Newsome, S.D., Gregg, J.W., 2005. Combining sources in stable isotope mixing models: alternative methods. Oecologia 144, 520–527.
Price, N.J., 1966. Fault and Joint Development in Brittle and Semi-brittle Rock, Pergamon Press, London, 176 p.

Ramsay, J.G., 1980. The crack-seal mechanism of rock deformation. Nature (London) 284, 135–139.
Reynolds Jr., R.C., 1992. X-ray diffraction studies of illite/smectite from rocks, <1 μm randomly oriented powders, and <1 μm oriented powder aggregates; the absence of laboratory-induced artifacts. Clays and Clay Minerals 40, 387–396.
Richards, I., Connelly, J., Gregory, R., Gray, D., 2002. The importance of diffusion, advection, and host-rock lithology on vein formation: a stable isotope study from the Paleozoic Ouachita orogenic belt, Arkansas and Oklahoma. Bulletin of the Geological Society of America 114, 1343–1355.
Rutter, E.H., 1983. Pressure solution in nature, theory and experiment. Journal of the Geological Society 140, 725–740.
Rye, D.M., Bradbury, H.J., 1988. Fluid flow in the crust: an example from a Pyrenean thrust ramp. American Journal of Science 288, 197–235.
Saffer, D.M., Tobin, H.J., 2011. Hydrogeology and mechanics of subduction zone Forearcs: fluid flow and pore pressure. Annual Review of Earth and Planetary Sciences 39, 157–186.
Sample, J.C., 2010. Stable isotope constraints on vein formation and fluid evolution along a recent thrust fault in the Cascadia accretionary wedge. Earth and Planetary Science Letters 293, 300–312.
Schmoker, J.W., Gautier, D.L., 1989. Compaction of basin sediments; modeling based on time-temperature history. Journal of Geophysical Research 94, 7379–7386.
Sibson, R.H., 1998. Brittle failure mode plots and extensional tectonic regimes. Journal of Structural Geology, 655–660.
Sleep, N., Blanpied, M.L., 1992. Creep, compaction and the weak rheology of major faults. Nature 359, 687–692.
Srodon, J., 1984. X-ray powder diffraction identification of illitic materials. Clays and Clay Minerals 32, 337–349.
Srodon, J., Eberl, D.D., 1984. Illite. Micas. Reviews in Mineralogy 13, 495–544.
Srodon, J., Elsass, F., McHardy, W.J., Morgan, D.J., 1992. Chemistry of illite-smectite inferred from TEM measurements of fundamental particles. Clay Minerals 27, 137–158.
Stockmal, G.S., Beaumont, C., Nguyen, M., Lee, B., 2007. Mechanics of thin-skinned fold and thrust belts; insights from numerical models. Geological Society of America 433, 63–98. Special Paper.
Suter, M., 1980. Tectonics of the External Part of the Sierra Madre Oriental Foreland Thrust-and-fold Belt between Xilitla and the Moctezuma River (Hidalgo and San Luis Potosí States), 4. Revista - Instituto de Geología. 19–31.
Suter, M., 1984. Cordilleran deformation along the eastern edge of the Valles-San Luis Potosí carbonate platform, Sierra Madre Oriental fold-thrust belt, east-central Mexico. Geological Society of America Bulletin 95, 1387–1397.
Suter, M., 1987. Structural traverse across the Sierra Madre Oriental fold-thrust belt in east-central Mexico. Geological Society of America Bulletin 98, 249–264.
Sydney Jr., C., 1966. Handbook of Physical Constants (revised edition), 97. Geological Society of America/Memoir. 587.
Tada, R., Siever, R., 1989. Pressure solution during diagenesis. Annual Review of Earth and Planetary Sciences 17, 89–118.
Taylor, H.P., 1974. The application of oxygen and hydrogen isotope studies to Problems of hydrothermal Alteration and ore deposition. Economic Geology 69, 843–883.
Touret, J.L.R., 2001. Fluids in metamorphic rocks. Lithos 55, 1–25.
Travé, A., Labaume, P., Vergés, J., 2007. Fluid systems in foreland fold-and-thrust belts; an overview from the southern Pyrenees. In: Lacombe, O., Lave, J., Roure, F., Vergés, J., Brun, J.P., Oncken, O., Weissert, H., Dullo, C. (Eds.), Thrust Belts and Foreland Basins; from Fold Kinematics to Hydrocarbon Systems. Springer.
Valencia-Islas, J.J., 1996. Implicaciones de la historia termica de la plataforma Valles-San Luis Potosí en la distribucion de los hidrocarburos y yacimientos minerales. Boletín de la Asociación Mexicana de Geólogos Petroleros 45, 1–19.
Vennemann, T.W., O'Neil, J.R., 1993. A simple and inexpensive method of hydrogen isotope and water analyses of minerals and rocks based on zinc reagent. Chemical Geology 103, 227–234.
Von Huene, R., Lee, H., 1982. The possible significance of pore fluid pressures in subduction zones; Studies in continental margin geology. AAPG Memoir 34, 781–791.
Vrolijk, P., Myers, G., Moore, J.C., 1988. Warm fluid migration along tectonic melanges in the Kodiak accretionary complex, Alaska. Journal of Geophysical Research 93, 10,313–10,324.
Warr, L.N., Rice, A.H.N., 1994. Interlaboratory standardization and calibration of clay mineral crystallinity and crystallite size data. Journal of Metamorphic Geology 12, 141–152.
Wassenaar, L.I., van Wilgenburg, S.L., Larson, K., Hobson, K.A., 2009. A groundwater isoscape $\delta D^{18}O$ for Mexico; Isoscapes; isotope mapping and its applications. Journal of Geochemical Exploration 102, 123–136.
Weaver, C.E., Grim, R.E., Guven, N., 1979. Bentonites; geology, mineralogy, properties and use; book review. Sedimentary Geology 24, 324–325.
Weissert, H., Erba, E., 2004. Volcanism, CO2 and palaeoclimate: a late jurassic-early cretaceous carbon and oxygen isotope record. Journal of the Geological Society of London 161, 695–702.
Weissert, H., Lini, A., Föllmi, K.B., Kuhn, O., 1998. Correlation of Early Cretaceous carbon isotope stratigraphy and platform drowning events: a possible link? Palaeogeography, Palaeoclimatology, Palaeoecology 137, 189–203.
Yeh, H.W., 1980. D/H ratios and late-stage dehydration of shales during burial. Geochimica et Cosmochimica Acta 44, 341–352.
Zheng, Y.F., 1994. Oxygen isotope fractionation in carbonate and sulfate minerals. Geochemical Journal 33, 109–126.